SEISMIC BEHAVIOUR AND NONLINEAR MODELING OF REINFORCED CONCRETE FLAT SLAB-COLUMN CONNECTIONS

by

Omar AlHarras

BEng (Hons), Loughborough University, 2013

A THESIS SUBMITTED IN PARTIAL FULFILLMENT OF

THE REQUIREMENTS FOR THE DEGREE OF

MASTER OF APPLIED SCIENCE

in

THE FACULTY OF GRADUATE AND POSTDOCTORAL STUDIES

(Civil Engineering)

THE UNIVERSITY OF BRITISH COLUMBIA

(Vancouver)

August 2015

Abstract

The contemporary structural design practice of tall buildings typically incorporates a lateral force resisting system, along with a gravity system that often includes reinforced concrete flat slabs. A major challenge with the design of this system is ensuring adequate strength and deformation capacities of the flat slab-column connections, especially when the structure is prone to strong seismic excitations. When a flat slab-column connection is subjected to a combination of gravity and lateral loads, failure may occur in multiple modes. Comprehensive literature reviews of the experimental studies and the analytical models related to reinforced concrete flat slabs, and flat slab-column connections are presented in *Chapters 2 and 3*, respectively.

The existing nonlinear models that are currently available in literature were developed as assessment tools for old flat-plate structures. Thus, they are not capable of capturing the hysteretic behaviour of ductile flat slab-column connections with shear reinforcement. In *Chapter 4*, a new nonlinear model for flat slab-column connections is proposed. Utilizing the proposed model allows detecting potential failures due to all the possible modes of failure. The model was verified and calibrated using data from actual experimental studies.

Chapter 5 investigates the effects of flat slabs on the global seismic response of typical high-rise concrete shear wall buildings. Two analytical case studies were conducted using a prototype building designed in Vancouver, Canada. The results from nonlinear dynamic analyses confirmed that including flat slabs in the analysis models of tall buildings is important to obtain accurate estimates of the structural responses and seismic demands. A concise summary of the research outcomes is presented in *Chapter 6*.

Preface

The author of this thesis was responsible for the literature review, model development, data processing, and presentation of results.

The design of the prototype building, as well as the selection and scaling of ground motions utilized in Chapter 5 were provided by Dr. Tony Yang, Jeremy Atkinson, and Stanley Chan. The design of the flat slab systems was done by the author of the thesis.

Parts of the work included in Chapter 4 have been presented at the 5th Tongji-UBC Symposium on Earthquake Engineering held in Shanghai, China in May 2015.

Table of Contents

List of Tables

List of Figures

List of Abbreviations

EBWM	:	Effective Beam Width Model
EFM	:	Equivalent Frame Model
FSC	:	Flat Slab-Column
GS	:	Gravity System
GM	:	Ground Motion
ISD	:	Inter-storey Drift
RC	:	Reinforced Concrete
RCFS	:	Reinforced Concrete Flat Slab
SFRS	:	Seismic Force Resisting System

Acknowledgements

First and foremost, I would like to thank my supervisor, Dr. Tony Yang, for his guidance, encouragement, and contributions. Dr. Yang has a great passion for pushing the innovation boundaries in structural and earthquake engineering, it has truly been a pleasure being part of his research team.

I would like to extend my special thanks to my colleagues and friends, in particular Lisa Tobber, Yuanjie Li, and Jeremy Atkinson for providing technical support and valuable input into my research.

Finally, I would like express my gratitude for my family, Kendra, and my wonderful friends at Green College.

Dedication

To my parents

Chapter 1: Introduction

1.1 Problem Statement

The current structural design practice of reinforced concrete buildings in seismically active regions typically incorporates a seismic force resisting system (SFRS), along with a gravity system (GS) which often includes flat slabs. The reinforced concrete flat slab (RCFS) system is a highly efficient floor system and is, therefore, very popular in high-rise construction in North America. Besides achieving a fast construction cycle time (often 5 to 6 days per floor), a 200 mm thick reinforced concrete flat slab can be designed to span a distance of 6 to 8 meters in typical residential or commercial buildings.

Ensuring adequate strength and deformation capacities of flat slab-column (FSC) connections is a major design challenge with the RCFS system, especially when the structure is prone to strong earthquake excitations. When a FSC connection is subjected to a combination of gravity load and unbalanced moments, failure may occur due to either punching shear, or exhausting the flexural capacity of the connection.

Traditional design procedures start with designing the SFRS to have sufficient strength and ductility to resist the expected seismic demands. Upon estimating lateral inter-storey drifts from the analysis of the SFRS, the GS elements are designed accordingly for drift-induced demands. The following flowchart summarizes a typical design process of FSC connections, as part of the GS:

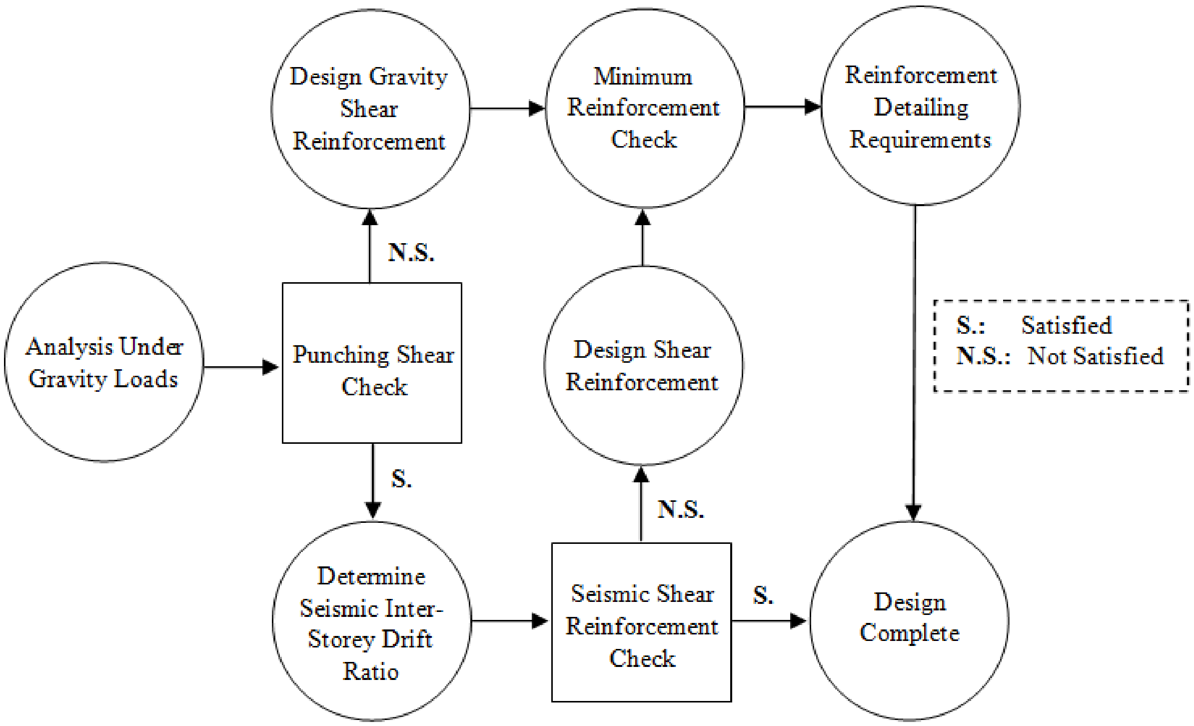

Figure 1-1: Typical Design Porcess of Flat Slab-Column Connections

This traditional approach may lead to unsafe designs due to ignoring the interaction between the SFRS and the GS, especially in tall buildings. Therefore, including flat slabs in the analysis model is important to capture this interaction between the SFRS and gravity columns. It is also to obtain realistic estimates of the lateral stiffness, inter-storey drifts, force demands, and energy dissipation. Thus, with increasing trends in performance-based design and assessment, developing a robust nonlinear finite element model for the RCFS system crucial to obtain accurate structural responses from time-history dynamic analyses.

1.2 Motivation

Several nonlinear modeling techniques of FSC connections have been developed in the past (e.g. by Hueste and Wight, 1999; Kang et al., 2009). However, these analytical models were developed as assessment tools for old flat-plate structures, where ductile FSC connections with shear reinforcement were not considered.

Figure 1-2 shows the recorded force-deformation data from experimental tests on two FSC connections conducted by Park et al. (2011). Both specimens have identical geometry, material properties, longitudinal reinforcement, and loading conditions. One of the specimens, however, contains shear reinforcement while the other does not. The cyclic response of the specimen with shear reinforcement indicate much improved strength capacity, ductility, and energy dissipation in comparison to the specimen without shear reinforcement. Hence, it could be concluded that the models proposed in the past for FSC connections are not appropriate to accurately simulate the hysteretic behaviour of ductile FSC connections with shear reinforcement.

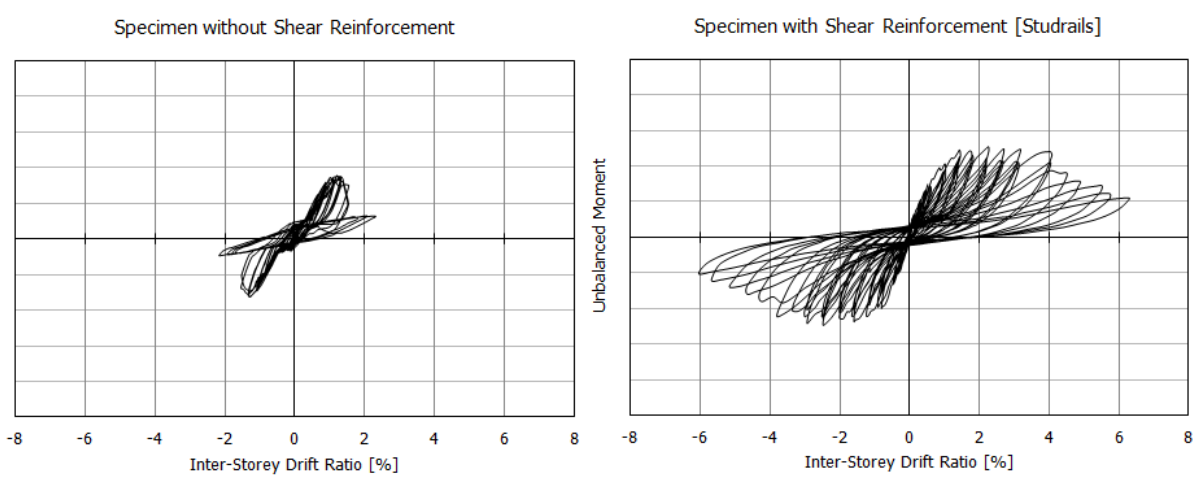

Figure 1-2: Comparison between the Hystretic Response of Non-ductile and Ductile FSC Connections - Experimental data by Park et al. (2011)

Therefore, a new nonlinear model that is capable of capturing the hysteretic behaviour of ductile FSC connections, accounting for all the possible failure modes was developed.

1.3 Goals and Objectives

This research project aims to contribute to the state of nonlinear modeling and performance-based assessment of reinforced concrete buildings with RCFS systems. This is achieved through:

- Providing a compilation of experimental studies to understand the seismic behaviour of FSC connections.
- Conducting a critical review of the existing analytical models and the provisions by the codes of practice related to FSC connections.
- Proposing a new nonlinear model that is capable of accurately simulating the hysteretic response of ductile reinforced concrete FSC connections, and capture potential shear or flexural failures.
- Investigating the effect of the RCFS system on the global seismic response of a typical high-rise shear wall building.

1.4 Thesis Outline

The seismic behaviour and nonlinear modeling of FSC connections are discussed in the following chapters:

Chapter (2): Provides a review of the experimental studies on flat slabs and FSC connections. The selected studies include various types of test specimens, with particular focus on slabs that contain shear reinforcement. At the end of the chapter, a summary of the experimental research outcomes is presented.

Chapter (3): Provides a review of the analytical models and design methods related to flat slabs and FSC connections. The chapter is divided into three main sections: [1] Strength models, [2] Lateral stiffness models, and [3] Models for drift-induced punching shear. Within each section, the relevant provisions from North American codes of practice, e.g. CSA A23.3 (2014) and ACI 318 (2014), are discussed.

Chapter (4): Presents a state-of-the-art lumped-plasticity modeling technique for the RCFS system. In addition, a new model to simulate the hysteretic flexural behaviour of ductile FSC connections is introduced. The proposed model is verified and calibrated using data from experimental tests on FSC subassemblies with different types of shear reinforcement. The model has been implemented in the OpenSees computational platform (PEER, 2015a) to be utilized in further applications.

Chapter (5): A tall reinforced concrete shear wall building with flat-plate gravity framing located in Vancouver, Canada was designed using a performance-based approach. Time-history dynamic analyses were conducted using strong ground motions to study the seismic performance of the building. Utilizing the model proposed in *Chapter 4*, two case studies were conducted. The studies aim to: [1] investigate the impact of including flat slabs in the analysis model on the global behaviour of tall shear wall buildings; [2] investigate the effect of different flat slab designs on the seismic response of the prototype building.

Chapter (6): Presents a summary of the research findings as well as recommendations for future research.

Chapter 2: Experimental Studies

2.1 Overview

Many experimental studies have been conducted over the past few decades to investigate the seismic behaviour of reinforced concrete FSC connections, both with and without shear reinforcement. When a FSC connection is subjected to a combination of gravity load, and unbalanced moments resulted from earthquake excitations, failure may occur due to:

- Punching shear, which could be stress-induced or drift-induced, and/or;
- Exhausting the flexural capacity of the slab within the connection's flexure-transfer width, which a ductile failure mechanism.

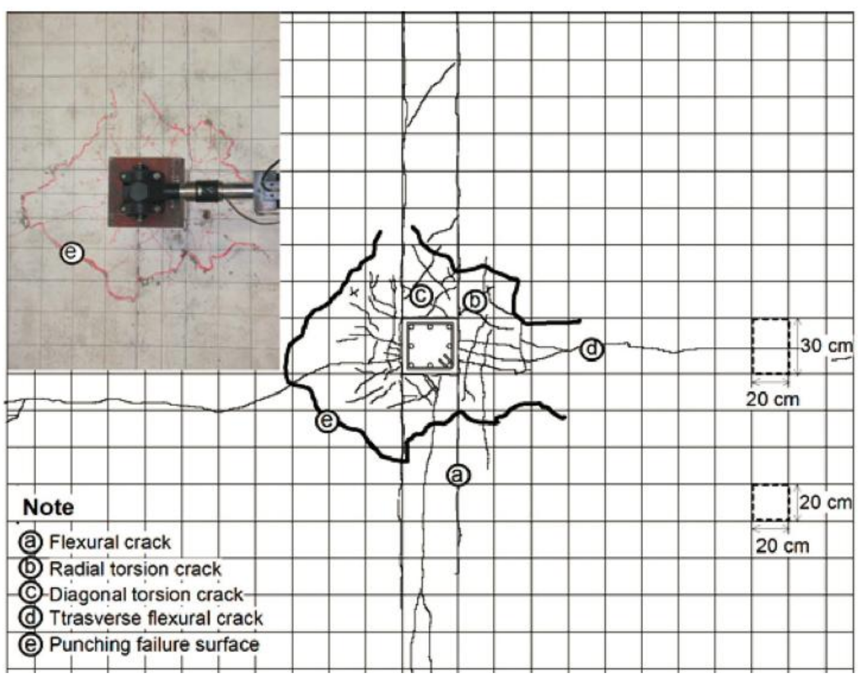

Figure 2-1: A Typical Crack Pattern of an Interior FSC Connection - Elevation View (Han et al., 2009)

Punching shear is a brittle failure mechanism that may eventually lead to progressive collapse if it occurs at multiple FSC connections in a building. This failure is observed when the stress in the joint's compression zone exceeds the capacity (Broms, 1990 and 2000). On the other hand, exhausting the flexural capacity is a ductile mechanism and is therefore preferred when as a governing failure mode when designing flat-plate structures in seismic zones. In experimental tests, the mode of failure can be identified by the type of observed cracks as well as the recorded force-deformation response of the test specimen. Typical crack patterns are illustrated in Figure 2-1.

The majority of experimental studies on FSC connections have been conducted following a typical procedure. A prototype multi-storey building with a RCFS system is designed in accordance with contemporary codes of practice, such as CSA A23.3 or ACI 318. A typical interior, edge, or corner connection (see illustration in Figure 2-2) is then selected and scaled down. Scale factors of 1/2 or 2/3 are common for this type of experiments for feasibility and economic purposes.

Objectives of experimental studies generally include:

- Investigating how unbalanced moments are transferred between flat slabs and the supporting columns in flexure and shear.
- Investigating the impact of post-tensioning and reinforcement detailing on the seismic behaviour of FSC connections.
- Investigating the impact of design parameters, such as the gravity shear ratio, the strength of concrete, or the amount of shear reinforcement on the hysteretic response of FSC connections.

- Investigating the effect of different types of shear reinforcement on the strength and ductility of typical FSC connections.
- Verifying analytical strength and stiffness models, and values of theoretical coefficients.

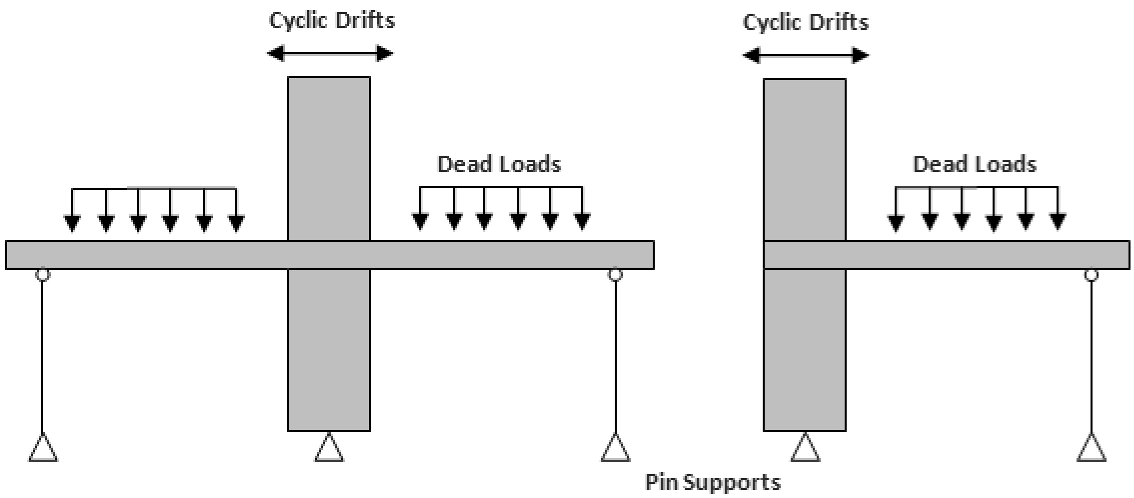

Figure 2-2: Typical Experimental Test Arrangements

In the following sections, selected experimental studies are summarized. Brief descriptions of test setups and specimens are provided, followed by the major findings of each study. The selected studies mainly focus on reinforced concrete FSC connections with shear reinforcement. Other studies on FSC connections without shear reinforcement, and post-tensioned concrete connections are included due to their important findings that contributed toward the evolution of analytical methods or code provisions.

2.2 Studies on Reinforced Concrete Flat Slab-Column Connections

Hawkins et al. (1975):

Hawkins et al. (1975) conducted one of the early studies on the cyclic behaviour of FSC connections with shear reinforcement. The experimental program included several FSC subassemblies both with and without stirrup reinforcement. The test specimens were subjected to combined gravity loads and lateral cyclic drifts in one direction.

The study concluded that the specimens with properly detailed stirrup reinforcement behaved in a ductile manner, with improved residual shear strength in comparison to the specimens without shear reinforcement. In addition, the recorded force-deformation responses indicated that the specimens with stirrups were dominated by flexural behaviour, which resulted in substantial increase in energy dissipation.

Test observations showed that the flexural behaviour of FSC connections is improved when the longitudinal reinforcement is placed within the vicinity of the column, especially for specimens with low reinforcement ratios.

Pan and Moehle (1992):

Pan and Moehle (1992) investigated the ductility, drift capacity, and seismic performance of FSC connections with different gravity shear ratios ($V_u/\phi V_c$). The experimental program consisted of five specimens without shear reinforcement, three of which were subjected to bi-directional lateral loads while the other two were subjected to lateral loads in only one direction.

One of the specimens was repaired using epoxy-grout after failure was detected. The specimen was retested in order to evaluate the effectiveness of FSC connection repairs.

The specimens loaded bi-directionally were found to exhibit reduced strength, drift capacity, and lateral stiffness compared to the specimens loaded in one direction. Similarly, increased gravity shear ratios resulted in weaker performance, with punching shear failure occurring at lesser drifts.

The test results of the repaired specimen did not show the anticipated performance except for the drift capacity which was almost totally regained. Hence, grouting was found not to be an effective retrofitting solution to regain the strength and the lateral stiffness of damaged FSC connections.

Robertson and Durrani (1993):

Robertson and Durrani (1993) conducted tests on three two-bay FSC subassemblies without shear reinforcement. The major objective of the tests was to investigate the effect of gravity shear ratio on the seismic behaviour of interior FSC connections. The same lateral cyclic drifts were applied to the three test specimens, while subjected to different levels gravity loading.

The recorded test results confirmed that with increased gravity shear ratios, the strength, maximum drift, and lateral stiffness of the FSC connections were significantly decreased. This is due to the accelerated crack propagation which led to brittle punching shear failures eventually. The test results confirmed the outcomes from Pan and Moehle's study in 1992.

Megally and Ghali (2000):

The experimental study by Megally and Ghali (2000) focused on the effectiveness of shear studs (or headed shear reinforcement) on the performance of FSC connections. Five geometrically identical edge FSC subassemblies with varying gravity shear ratios were tested under cyclic loading. One of the specimens did not contain shear reinforcement, while the other four specimens had different arrangements of shear studs, i.e. different s/d ratios (spacing-to-effective depth ratios) as illustrated in Figure 2-3.

The recorded force-deformation responses of the tested specimens indicated that using shear studs drastically improved the ductility and the maximum inter-storey drift ratios achieved by the FSC connections. Similarly to FSC connections without shear reinforcement, a direct relationship between the gravity shear ratio $\left(V_u/\phi V_c\right)$ and the lateral drift capacity of the tested specimens was found. Hence, it was concluded that punching shear failure at a FSC connection with shear studs is expected to occur at a lower inter-storey drift ratio if the gravity shear ratio is increased.

Spacing of the shear studs was found not to have a significant impact of the performance of FSC connections. Yet, the results showed that reducing the spacing between studs from $0.75d$ to $0.44d$ lead to a minimal improvement of the drift capacity and ductility of the connections.

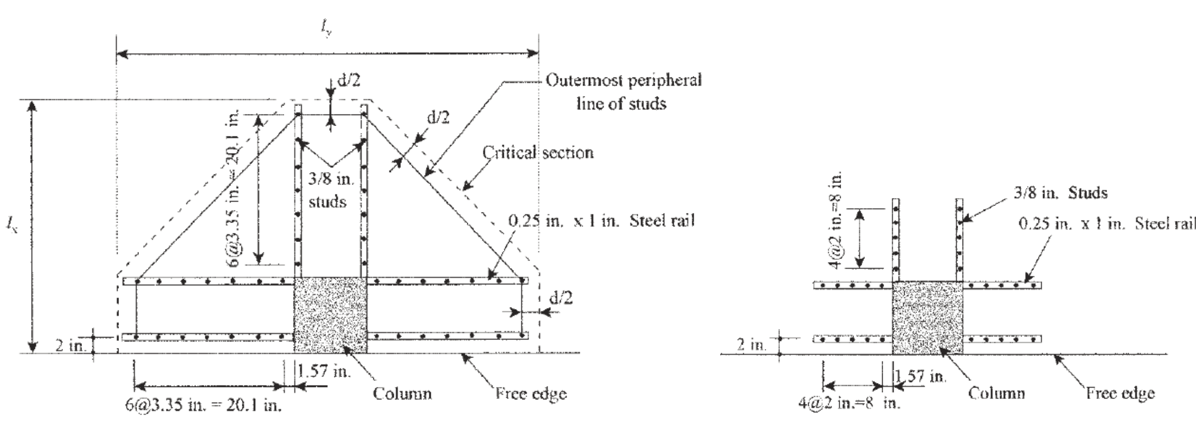

Figure 2-3: Arrangements of Shear Studs Used in Megally and Ghali's (2000) Experimental Study

Hwang and Moehle (2000a):

Hwang and Moehle (2000a) conducted an experimental study on a two-way flat slab with multiple spans, supported by columns with different geometries (see Figure 2-4). The test aimed to investigate the lateral stiffness of the slab in both directions, and the seismic behaviour of interior and exterior FSC connection. Different longitudinal reinforcement detailing was used for the FSC connections to investigate the suitability of typical design practices. The test specimen was subjected to cyclic bi-directional lateral drifts in addition to a constant gravity load.

The test results validated the EBWM and the EFM models used to estimate the lateral stiffness of flat slabs (the stiffness analytical models are discussed in further detail in Section 3.3). Different reinforcement were found not to have a significant impact of the seismic behaviour of FSC connections. However, the FSC connections with continuous bottom reinforcement did not collapse after the occurrence of punching shear, unlike those without bottom reinforcement passing through the columns.

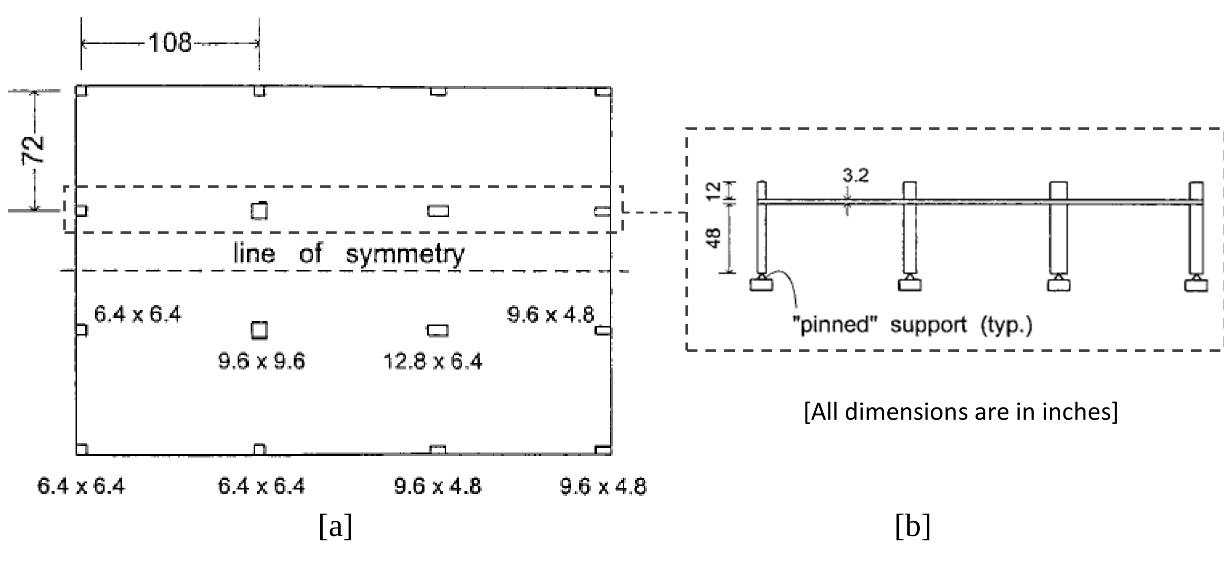

Figure 2-4: Nine-panel Frame Test Specimen by Hwang and Moehle (2000a)

El-Salakawy et al. (2000):

Floor openings next to columns are often utilized for running building services across building floors. El-Salakawy et al. (2000) experimentally investigated the behaviour of exterior FSC connections with adjacent floor openings. The experimental program consisted of eight large-scale specimens, four of which contained stud rails as shear reinforcement (see Figure 2-5).

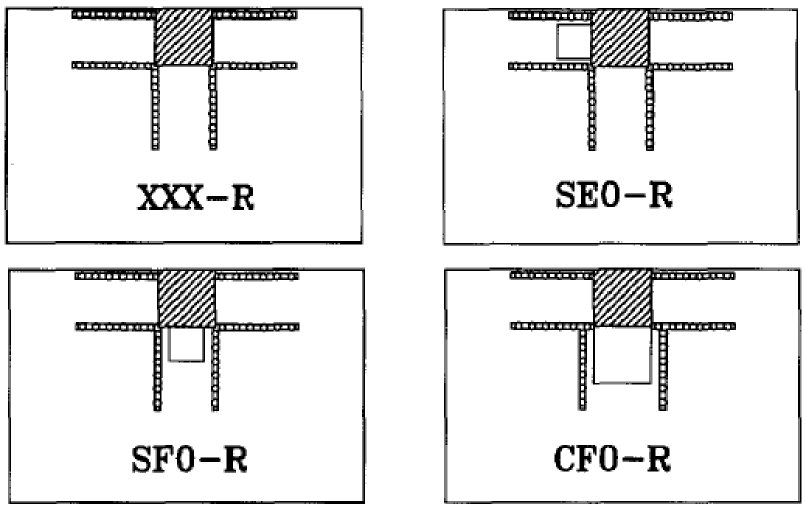

Figure 2-5: Plan View of Test Specimens with Shear Reinforcement (El-Salakawy et al., 2000)

From the recorded force-deformation data of the eight specimens, it was concluded that the existence of floor openings, regardless of their locations, decreases the lateral stiffness of FSC connections. However, specimens with shear reinforcement suffered less reduction in the lateral stiffness and the unbalanced moment transfer capacity. Moreover, it was found that floor openings on the sides of columns have less impact on the seismic performance of FSC connections than openings located in front of columns. One of the specimens with shear reinforcement (CF0-R) failed in a punching shear mechanism. Hence, the study recommends that floor openings as large as the column width shall not be constructed in flat slabs, even if shear reinforcement is provided.

Robertson et al. (2002):

Robertson et al. (2002) conducted an extensive experimental study on interior FSC connections with multiple types of shear reinforcement (single-leg stirrups, closed-hoop stirrups, and shear studs). The specimens had different gravity shear ratios, and were subjected to a cyclic lateral load in one direction. For comparison purposes, an additional control specimen without shear reinforcement was tested under the same lateral loading protocol.

The specimens with shear reinforcement showed substantially enhanced ductility, reaching a lateral inter-storey drift ratio of up to 8% without failing in punching shear. In contrast, the control specimen without shear reinforcement suffered a punching shear failure during the 3.5% drift cycle. The test results also indicated that the specimens with shear reinforcement resisted up to 22% greater peak unbalanced moment compared to the control specimen.

The experimental results confirmed the outcomes from preceding experimental studies on FSC connections with shear reinforcement (e.g. by Hawkins et al., 1975; Islam and Park, 1976; Elgabry and Ghali, 1987; Dilger and Cao, 1992; Dilger and Brown, 1995; Megally and Ghali, 2000).

Kang and Wallace (2005, 2006):

Shake table tests were conducted by Kang and Wallace (2005) on multi-bay FSC frames, with both reinforced concrete and post-tensioned concrete slabs. The specimens included FSC connections with and without shear reinforcement. The test specimens were subjected to dynamic, earthquake-type loading in one direction as well as variable gravity shear ratios.

The test results verified two analytical assumptions that are common in practice:

- A flexural-transfer width of $(c_2 + 3h)$ is a appropriate for estimating the flexural capacity of both interior and exterior FSC connections. This was proven from the reinforcing bar strains and the slab curvature data, which showed that the yielding of longitudinal reinforcement only occurred within the assumed flexural-transfer width at each connection.
- Using the effective beam width model is sufficient estimate the elastic lateral stiffness of flat slabs (the stiffness analytical models are discussed in further detail in Section 3.3).

Similar to the observations by Megally and Ghali (2000), the experimental results from shake table tests showed a relationship between the gravity shear ratio and the lateral inter-storey drift ratio at which punching shear occurs. However, results from the dynamic tests suggest lower drift capacity than those suggested by quasi-static tests. In a latter study by Kang and Wallace (2006), a model for drift-induced punching shear was proposed based on compiled results from various experimental studies (discussed in further detail in Section 3.4).

Park et al. (2007, 2011):

Lattice reinforcement was proposed by Park et al. (2007) as a new type of shear reinforcement for FSC connections (see Figure 2-6). The primary concept behind developing this type of shear reinforcement is engaging steel bars (ϕ5) in truss-action and dowel-action mechanisms to resist punching shear. Two sets of experimental programs were conducted by Park et al. (2007, 2011) in which the performance of FSC connections with lattice reinforcement were compared to the performance of connections with other types of shear reinforcement.

The results from the 2007 study proved that lattice reinforcement significantly improves the cyclic performance of FSC connections. It was observed that the strength of connections with lattice reinforcement were maintained up to 9.2 times the deformation capacity of identical connections without shear reinforcement, even after the cracking and crushing of concrete.

Figure 2-6: Lattice Reinforcement for FSC Connections (Park et al., 2007)

The 2011 study comprised of twelve specimens tested under cyclic lateral loading in one direction. The experimental test results proved that the specimens with lattice reinforcement showed better strength and deformation capacities, in addition to greater energy dissipation in comparison to the specimens with other types of shear reinforcement.

Rha et al. (2014):

Rha et al. (2014) conducted experimental tests on five multi-bay FSC frames (see Figure 2-7) with different longitudinal reinforcement configurations. The specimens were subjected to gravity loads as well as lateral cyclic drifts in one direction. The test setup simulated actual boundary conditions similar to those in real buildings by extending the column heights above the slab level.

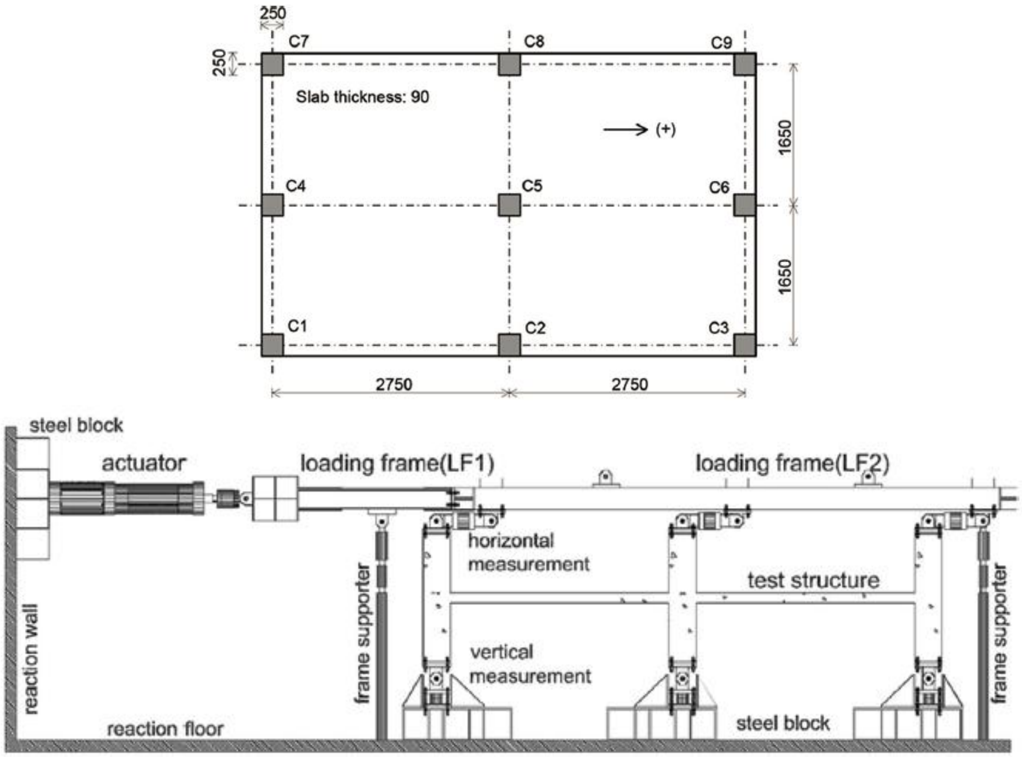

Figure 2-7: Layout of a Typical Test Specimen and Test Setup (Rha et al., 2014)

The recorded test data suggested that there is no interaction between shear transfer and moment transfer at edge FSC connections. This is because the unbalanced moments applied to the edge connections were almost fully transferred in flexure, with negligible eccentric shear stresses induced. This observation confirms conclusions drawn from preceding studies by Moehle (1988) and Kang and Wallace (2005). The test results also indicated that the FSC connections with increased continuous bottom reinforcement ratios showed improved strength and ductility.

2.3 Summary of the Outcomes from Experimental Studies

- When a FSC connection is subjected to a combination of gravity load and seismic deformations, failure may occur due to either: [1] punching shear, or [2] exhausting the flexural capacity of the slab within the flexure-transfer width.

- Shear reinforcement significantly improves the seismic performance of FSC connections in terms of strength capacity, ductility, stiffness degradation, and energy absorption. Experimental studies have investigated the behaviour of interior and exterior FSC connections with multiple types of shear reinforcement. Shear studs and lattice reinforcement were proven to be more effective than stirrups for enhancing the seismic response of FSC connections.

- Flexural yielding of the longitudinal reinforcement will occur prior to punching shear failure if the FSC connection is designed with adequate shear reinforcement. Reinforcing bar strains and slab curvature data from both static cyclic tests and dynamic shake table tests indicate that a flexure-transfer width of $c_2 + 3h$ is appropriate for estimating the flexural capacity of both interior and exterior connections.

- Results from experimental studies on multi-bay specimens demonstrate that flat slabs have true lateral elastic stiffness values less than those theoretically estimated based on full slab widths. Steady stiffness degradation is also observed with increasing inter-storey drifts due to the propagation of cracks while subjected to gravity and lateral loads and lateral drifts.

- The interaction between unbalanced moment and shear at edge FSC connections is negligible. This indicates that when an unbalanced moments is applied to an edge FSC connections, it is almost fully transferred in flexure. The related provisions in ACI 318 (2014) account for this behaviour (further discussion is provided in Section 3.2.1.3).

- Placing floor openings adjacent to FSC connections is not recommended for structures in seismic zones. Floor openings lead to a significant decrease in the strength capacity of FSC connections, which may lead to potential punching shear failures.

- Detailing of the slab's longitudinal reinforcement does not have a significant impact of the performance of FSC connections. However, placing of continuous bottom reinforcement at interior connections reduces the risk of progressive collapse during severe earthquakes.

Chapter 3: Analytical Models

3.1 Overview

Based on the results and observations from experimental studies, several analytical models related to the RCFS system have been developed over the past decades. Analytical models can be divided into two main categories: strength models and stiffness models. In this chapter, a comprehensive review of these models is presented, along with critical discussions on the related provisions from the North American design codes: CSA A23.3 (2014) and ACI 318 (2014).

3.2 Strength Models

3.2.1 Eccentric Shear Stress Model

3.2.1.1 Principals

The eccentric shear stress model is the most popular numerical method to estimate the punching shear capacity of FSC connections subjected to a combination of a vertical load and an unbalanced moment.

The shear stress induced by the gravity load is referred to as the *direct shear stress*. The direct shear stress can be evaluated assuming a uniform stress distribution along the perimeter of the critical section (see Figure 3-1a). The applied unbalanced moment is assumed to be partially transferred in shear, while the remainder of the moment is transferred in flexure over the flexure-transfer width $\left(c_2 + 3h\right)$. The portion of the unbalanced moment transferred in shear is referred to as the *eccentric shear stress*, which is assumed to vary linearly at the sides of the critical section parallel to the unbalanced moment direction (see Figure 3-1b).

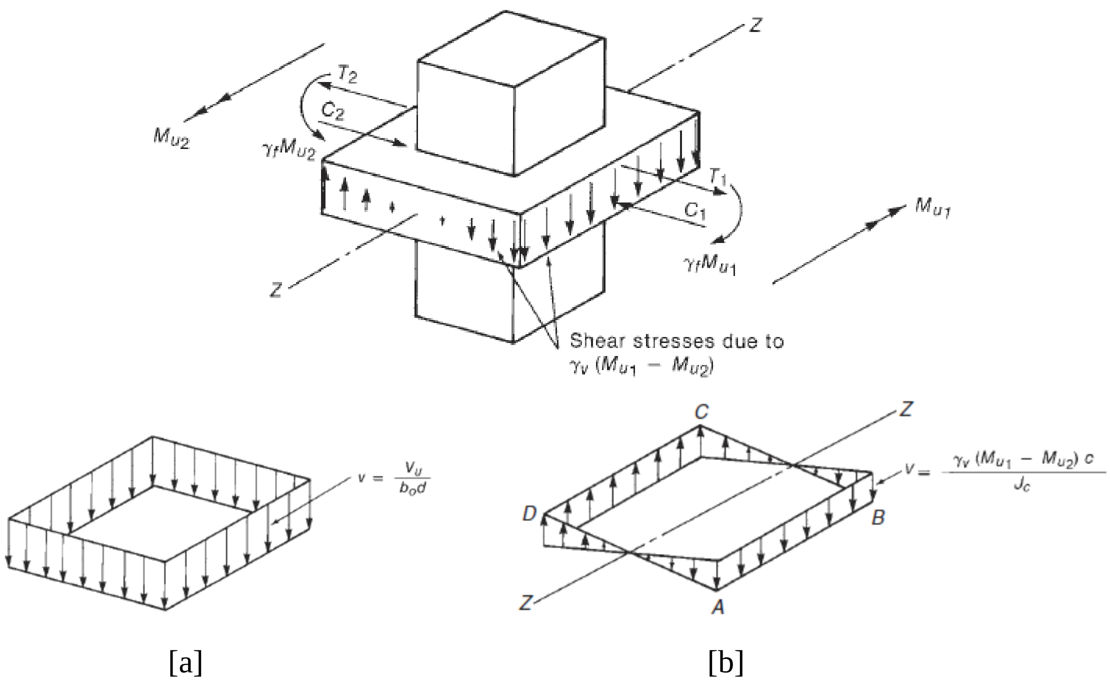

Figure 3-1: Shear Stresses at a FSC Connection due to [a] Gravity Loading and [b] Unbalanced Moment (Wight and MacGregor, 2012 [p.714])

In accordance with the North American design codes (e.g. Clause 13.3.3 in CSA A23.3-14), the critical section is taken at a distance of $d/2$ from each column face; where $d =$ the effective thickness of the slab (see Figure 3-2). The fractions of the unbalanced moment transferred by shear and by flexure are determined based on the empirical coefficients γ_v and γ_f , respectively, where:

$$\gamma_v + \gamma_f = 1.0 \qquad \textbf{Equation 3-1}$$

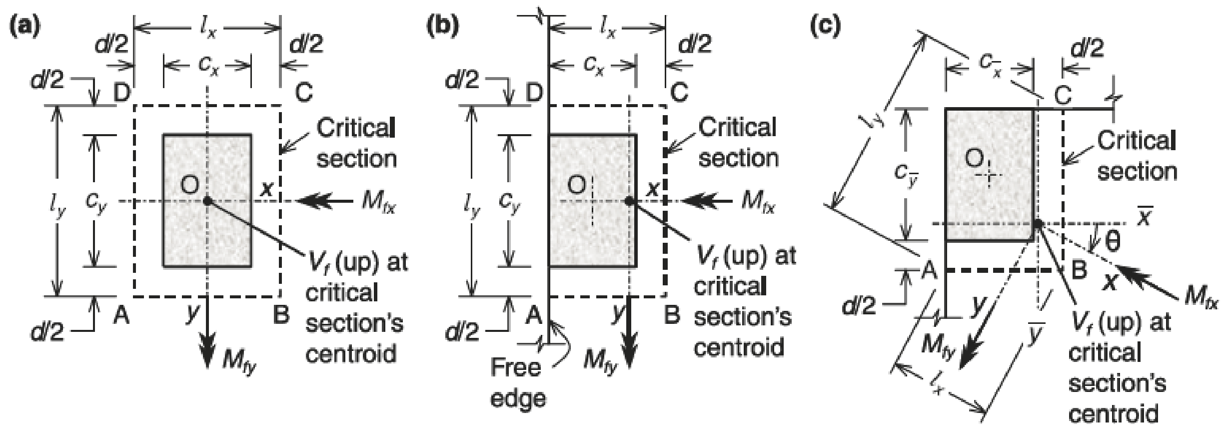

Figure 3-2: Shear Critical Sections around [a] Interior Column; [b] Edge Column; [c] Corner Column (Gayed and Ghali, 2008)

Thus, the maximum resultant shear stress due to both the direct shear stress and the eccentric shear stresses can be estimated as:

$$v_u = \frac{V_u}{A_c} + \gamma_{vx}\frac{M_{ux}y}{J_x} + \gamma_{vy}\frac{M_{uy}x}{J_y}$$ **Equation 3-2**

$$J_y = \frac{d(l_x^3)}{6} + \frac{d(l_y)(l_x^2)}{2} + \frac{(l_x)d^3}{6}$$ **Equation 3-3**

Equations 3-2 and 3-3 were proposed by Di Stasio and Buren (1960). The eccentric shear stress model was first verified by an extensive experimental study conducted by Hanson and Hanson (1968) that included 17 FSC connection specimens, all without shear reinforcement. Studies on connections with shear reinforcement were later conducted to further verify predictions based on this strength model (e.g. Elgabry and Ghali, 1996a; Ritchie et al., 2006).

3.2.1.2 Unbalanced Moment Transfer Factors

Other studies have further investigated the eccentric shear approach, some of which focused on determining appropriate values for the γ_v and γ_f factors. Initial code formulations suggested the following equations to obtain γ_v for unbalanced moments transferred about the principal axes of the supporting column:

$$\gamma_{vx} = 1 - \frac{1}{1 + (2/3)\sqrt{l_y / l_x}}$$ **Equation 3-4**

$$\gamma_{vy} = 1 - \frac{1}{1 + (2/3)\sqrt{l_x / l_y}}$$ **Equation 3-5**

where: l_x and l_y are the dimensions of the critical section as illustrated in Figure 3-3.

Equations 3-4 and 3-5 were derived based on studies on interior FSC connections without shear reinforcement. Later studies by Elgabry and Ghali (1996a; 1996b) proposed modified formulations to evaluate γ_v for other types of FSC connections that include edge connections, corner connections, and connections with shear reinforcement. The proposed modifications were based on finite element analyses calibrated to experimental data. The calculated shear stresses in Elgabry and Ghali's analyses are, however, obtained using the critical section's second moments of area, i.e. I_x and I_y instead of J_x and J_y. This simplification leads to ignoring the horizontal stresses induced by the transferred unbalanced moment, and considering only the induced vertical stresses. This assumption was justified since $\left(l_x d^3/6\right)$ and $\left(l_y d^3/6\right)$ usually have less than 3% contribution to the resultant shear stress from *Equation 3-2*.

$$\gamma_{vy} = 1 - \frac{1}{1 + (2/3)\sqrt{l_x / l_y - 0.2}} \qquad \text{when:} \quad l_x / l_y \geq 0.2 \qquad \textbf{Equation 3-6}$$

$$\gamma_{vy} = 0 \qquad \text{when:} \quad l_x / l_y < 0.2 \qquad \textbf{Equation 3-7}$$

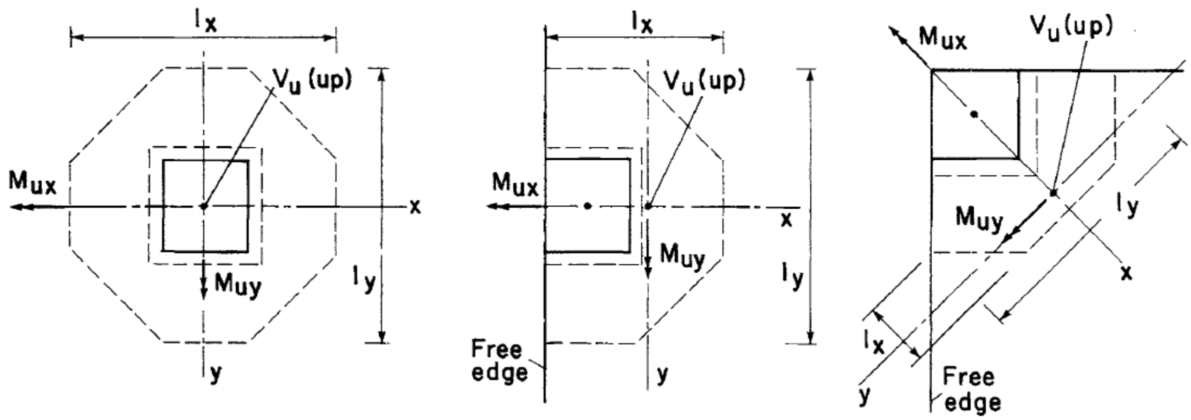

[a] [b] [C]

Figure 3-3: Critical Sections of [a] Interior Connections; [b] Exterior Connections; [c] Corner Connections (Elgabry and Ghali, 1996a)

Equations 3-6 and 3-7 are the modified formulae proposed by Elgabry and Ghali (1996a; 1996b) for edge connections. In case of FSC connections with shear reinforcement, the same equations can be used to evaluate γ_v at the critical section farther away from the column faces (see Figure 3-3). For corner connections, a constant factor γ_v of 0.4 in the direction lesser principal axis of the critical section was recommended. Complementary studies with extensive linear and nonlinear finite element analyses verified the above equations (e.g. Megally and Ghali, 1996; Gayed and Ghali, 2008).

An analytical study by Luo and Durrani (1994) proposed accounting for the top longitudinal reinforcement ratio when estimating the unbalanced moment transfer factors, γ_v and γ_f. Referring to results from experimental studies, Luo and Durrani observed that the portion of the unbalanced moment transferred in shear increases as the top longitudinal reinforcement ratio at the connection increases. Accordingly, they proposed *Equation 3-8* to estimate γ_v for interior connections:

$$\gamma_{vy} = 1.1 - 18\rho_{tc} - \frac{1}{1 + (2/3)\sqrt{l_x / l_y}} \qquad \textbf{Equation 3-8}$$

where: $\rho_{tc} =$ ratio of the top longitudinal reinforcement within the column strip.

3.2.1.3 Provisions by the Codes of Practice

The eccentric shear stress model was first adopted by ACI 318 in 1971, and has been implemented in several editions of CSA A23.3. The model is also utilized in other special publications on the design of FSC connections, such as ACI 421.2R (2010) and ACI 352.1R (2011).

CSA A23.3 (2014) state the following provisions to estimate the resultant shear stress at a FSC connection due to a gravity load and bi-directional unbalanced moments:

Clause 13.3.5.3; Clause 13.3.5.5	$v_f = \frac{V_f}{b_o d} + \left(\frac{\gamma_v M_f e}{J}\right)_x + \left(\frac{\gamma_v M_f e}{J}\right)_y$ $\gamma_v = 1 - \frac{1}{1 + (2/3)\sqrt{b_1 / b_2}}$

Similarly, but assuming the unbalanced moment in one principal direction at a time, ACI 318 (2014) expresses the resultant shear stress as:

Clause 8.4.4.2.3; Clause 8.4.2.3.2; Clause 8.4.4.2.2	$v_u = v_{ug} \pm \frac{\gamma_v M_{sc} c}{J_c}$ $\gamma_f = \frac{1}{1+(2/3)\sqrt{b_1/b_2}}$ $\gamma_v = 1-\gamma_f$

Therefore, the capacity needs to be made in both orthogonal principal directions using consistent load cases.

ACI 318-14 (Clause 8.4.2.3.4) and ACI 352.1R-11 (Clause 5.2.1.2) allow the calculated γ_f factors to be increased for non-prestressed slabs depending on:

- The location of the connection;
- The factored gravity shear ratio, and;
- The reinforcement tensile strain within the flexure-transfer width.

Applying an increased γ_f factor leads to a reduction in the estimated resultant shear stress (see *Equation 3-1*). However, these modifications are justified through test observations by Moehle (1988), Hwang and Moehle (1990), and Kang and Wallace (2006). In contrast, Gayed and Ghali (2008) argue that the gravity shear ratio has no relevance to the γ_v and γ_f factors, based on numerical analyses and different interpretations to Moehle's (1988) experimental test results. Thus, Gayed and Ghali recommend removing these clauses from ACI 318 and ACI 352.1R.

According to CSA A23.3 (2014), the punching shear resistance of FSC connections with shear reinforcement can be estimated by the following clauses:

Clause 13.3.7.3 Clause 13.3.8.2; Clause 13.3.9.3;	$v_r = v_c + v_s$ ▪ $v_f \le v_r$ ▪ $v_c = 0.28\lambda\phi_c\sqrt{f'_c}$ in case of using headed shear reinforcement. ▪ $v_c = 0.19\lambda\phi_c\sqrt{f'_c}$ in case of using stirrups shear reinforcement.

The corresponding provisions given by ACI 318 (2014) are:

Clause 22.6.1.3; Clause 22.6.6.1	$v_n = v_c + v_s$ ▪ $v_u \le \phi v_n$ ▪ $v_c = 0.25\lambda\sqrt{f'_c}$ in case of using headed shear reinforcement. ▪ $v_c = 0.17\lambda\sqrt{f'_c}$ in case of using stirrups shear reinforcement.

where: $v_c =$ shear resistance provided by reinforcement, $v_s =$ shear resistance provided by reinforcement, $\phi =$ material reduction factor defined by the adopted code, $\lambda =$ concrete density factor, and $f'_c =$ the specified compressive strength of concrete.

Results from experimental studies on RC flat slabs (by Mowrer and Vanderbilt, 1967; Ivy et al., 1969; Osman et al., 2000) indicated that slabs with light-weight concrete have lower punching shear resistance compared to slabs with normal-weight concrete. Therefore, a λ factor is specified in both codes in order to account for the effect of employing low-density aggregate in the concrete mix. A similar modification factor C_v is specified by ACI 352.1R (2011).

3.2.2 Idealized Resistance Mechanism Model

Based on a qualitative study of the global resistance mechanism of FSC connections (see Figure 3-4), an idealized model was proposed by Farhey et al. (1997). The model suggests three major contributors to the resistance of connections subjected to combined gravity and lateral loads:

- Torsional resistances at the side face of the column.
- Flexural resistances at both faces of the column in the direction of the applied unbalanced moment.
- Shear resistances transferred by the flexural compression areas.

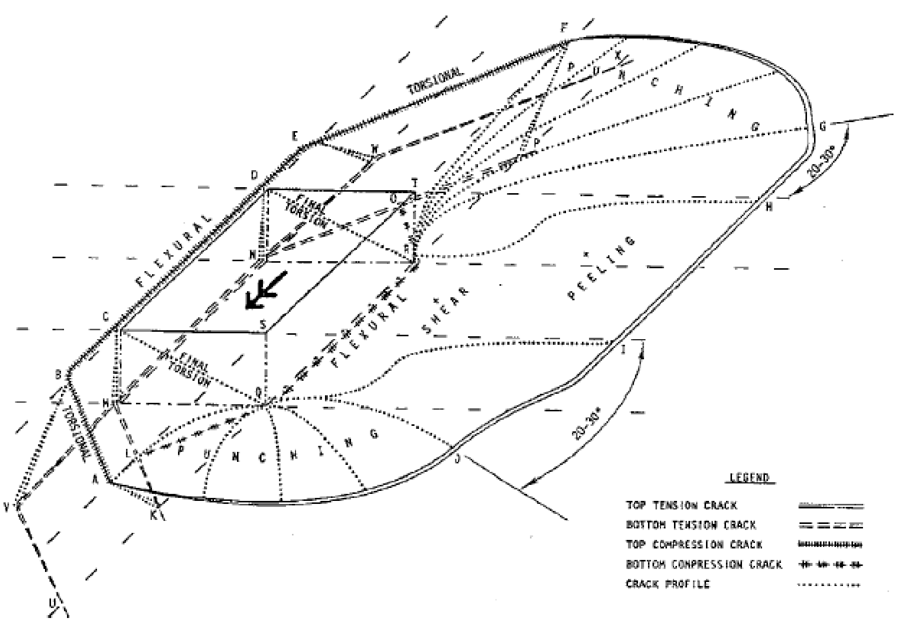

Figure 3-4: Idealized Ultimate Collapse Mechanisms (Farhey et al., 1997)

The model implements an analytical approach to estimate the ultimate torsional resistance component at the sides of the connection *(Equations 3-9 and 3-10).* The approach was proposed and experimentally verified by Marti et al. (1987a; 1987b).

$$T_u = f_y \sqrt{a_x a_y}\left[h - \frac{f_y}{0.45 f'_c}\left(a_x + a_y\right)\right]$$ **Equation 3-9**

such that: $$a_x \le \frac{1}{3}\left(0.45h\frac{f'_c}{f_y} - a_y\right)$$ **Equation 3-10**

where: $a_x =$ The cross-sectional area of lateral reinforcement per unit width, $a_y =$ the cross-sectional area of transverse reinforcement per unit length, $h =$ thickness of the slab, $f'_c =$ the specified compressive strength of concrete, and $f_y =$ the yield strength of reinforcement.

The twist at which the ultimate torque occurs is estimated by *Equation 3-11*:

$$\phi_u = \frac{0.1064 + 0.0152\rho_{TL}}{\left(1 - 0.63\frac{h}{c_1}\right)\frac{h}{6}}\left(1 + \frac{10}{h^2}\right)L_T$$ **Equation 3-11**

where: $\rho_{TL} =$ The section's total reinforcement ratio, $c_1 =$ side width of the column, and $L_T =$ length of the torsional collapse mechanism.

The flexural resistance components at the front and back faces of the column are inter-related due to the torsional mechanism. The flexural response at each face was found to be well represented by traditional sectional analysis, ignoring the steel reinforcement within the compression zone. The participating slab widths in flexure can be estimated as:

$$b_{front} = c_2 + 2\left(c_1 \cot \alpha_{u,bottom} + h\right)$$ **Equation 3-12**

$$b_{back} = c_2 + 2\left[c_1\left(\cot \alpha_{u,bottom} - \cot \beta_{top}\right) + 2h\right]$$ **Equation 3-13**

where: $$\alpha_u = \operatorname{arccot}\left[\frac{T_y}{a_x f_y c_1 h}\right]$$ **Equation 3-14** and: $$\beta = \text{arccot}\left[\frac{h}{c_1} + \cot\alpha_u\right]$$ **Equation 3-15**

where: $c_2 =$ width of front or back face the column, $\alpha_u =$ orientation of the torsional tension collapse cracks, and $\beta =$ orientation of the torsional compression collapse crack.

An equivalent moment is used to account for shear resistance components. The equivalent moment can be evaluated by *Equation 3-16*:

$$M_s = v_c + \left(\frac{c_1}{2}\right)\left(b_{front}c_{front} + b_{back}c_{back}\right)$$ **Equation 3-16**

Therefore, the global resistance of the FSC connection is estimated by summing the contributions of the three resistance components. An example comparison between the predicted strength and the experimental response of a FSC subassembly is shown in Figure 3-5.

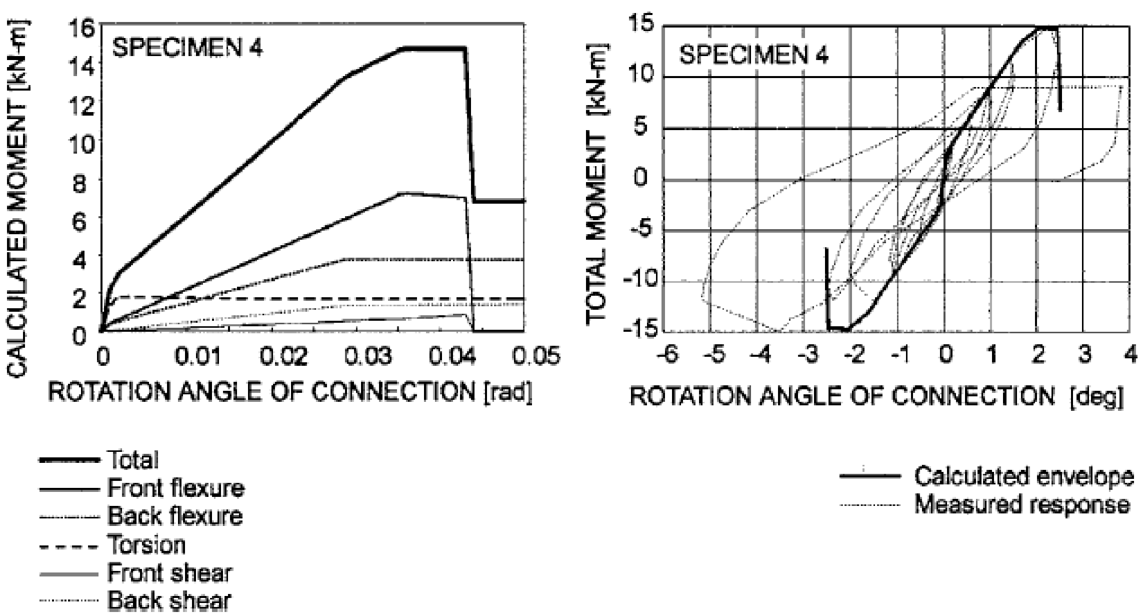

Figure 3-5: Comparison of Predicted and Measured FSC Capacities (Farhey et al., 1997)

3.2.3 Park and Choi's Model

Park and Choi (2006; 2007) and Choi et al. (2014a; 2014b) conducted a series of analytical studies to investigate the strength of reinforced concrete FSC connections and the distribution of the internal forces when subjected to unbalanced moments. The main motivation of the their studies was to obtain a design model that is capable of eliminating the uncertainties of the eccentric shear stress model, such as the distribution and strength of eccentric shear stresses, or the empirical estimations of the γ_v and γ_f factors.

Park and Choi's approach is somewhat similar to the philosophy of the model proposed by Farhey et al. (1997). The approach assumes that three resistance mechanisms, which can be expressed in terms of moment capacities, contribute to the total response of FSC connections (see Figure 3-6). Therefore, the nominal capacity a connection can be estimated such that:

$$M_n = M_F + M_S + M_T$$ **Equation 3-17**

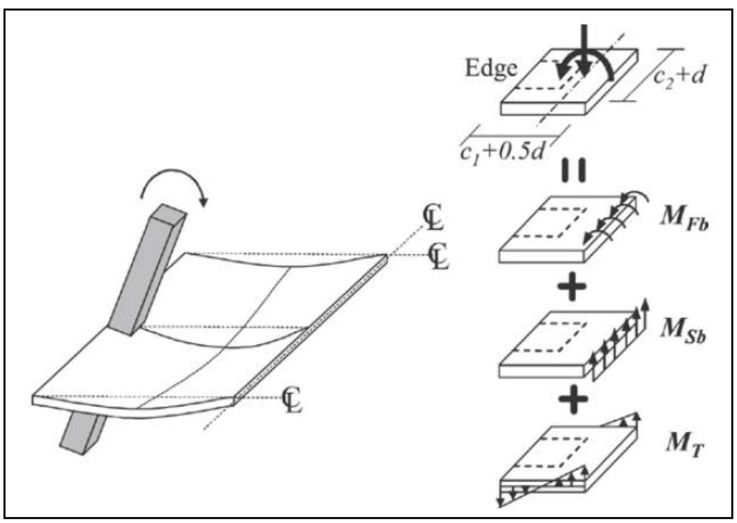

Figure 3-6: Resistance Mechanisms in an Exterior Slab-Column Connection (Park et al., 2006a)

For interior connections, the resistance components are estimated as:

$$M_F = A_{sf} f_y . jd + A_{sb} f_y . jd \qquad \textbf{Equation 3-18}$$

$$M_S = [(v_c - v_g)(c_2 + d)d](c_1 + d) \qquad \textbf{Equation 3-19}$$

$$M_T = \frac{4}{3}(v_{cT} - v_g)\left[\frac{c_1 + d}{2}\right]^2 d \geq 0 \qquad \textbf{Equation 3-20}$$

For exterior connections, the resistance components are estimated as:

$$M_F = A_{sf} f_y . jd \qquad \textbf{Equation 3-21}$$

$$M_S = 0.5 v_c (c_2 + d)(c_1 + d)d \qquad \textbf{Equation 3-22}$$

$$M_T = \left[c_{N2} + \frac{2}{3}c_{N1} - \frac{c_1}{2}\right] v_{cTf} c_{N1} d + \left[-\frac{1}{3}c_{N2} + \frac{c_1}{2}\right] v_{cTf} c_{N2} d \qquad \textbf{Equation 3-23}$$

where: $A_s =$ areas of the tensile reinforcement at the front or back of the critical section, $f_y =$ the yield strength of reinforcement, $jd =$ the cross-sectional lever arm, $v_c =$ the shear resistance provided by concrete, $v_g =$ the direct shear stress due to gravity load, $v_{cTf} =$ the shear stress capacity of the connection sides, $c_1 =$ side width of the column, $c_2 =$ width of front face the column, and $d =$ the effective depth of the slab.

c_{N1} and c_{N2} represent the distances from the neutral axis to the front and back faces of the critical section, respectively (see Figure 3-7). If $c_{N1} \geq c_{N2}$, the maximum side shear stress at the intersection with the front face $\left(v_{cTf}\right)$ is taken equal to v_c, while at the back face $\left(v_{cTb}\right)$ is taken equal to $\left(c_{N2}/c_{N1}\right)v_c$. In contrast, if $c_{N1} < c_{N2}$, v_{cTb} is taken equal to v_c, and v_{cTf} as $\left(c_{N1}/c_{N2}\right)v_c$.

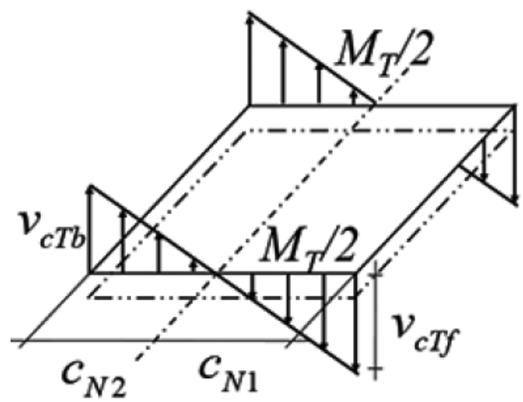

Figure 3-7: Torsional Shear Stress Distribution at the Critical Section of an Interior FSC Connections

The model was verified using data from 247 experiments on FSC connections. The numerical predictions obtained using the model showed good matches to the experimental results. However, the model has not yet been verified for FSC connections with shear reinforcement.

3.3 Lateral Elastic Stiffness Models

Appropriately estimating the elastic lateral stiffness and the stiffness degradation of flat slabs is essential to obtain realistic responses from numerical models of building with RCFS systems. Results from experimental studies on multi-bay specimens (by Hwang and Moehle, 2000a) indicated that RC flat slabs usually have true lateral elastic stiffness values less than those theoretically estimated based on full widths. Steady stiffness degradation is also observed with increasing inter-storey drifts due to the propagation of cracks. In order to account for this behaviour, researchers have proposed different models, the most popular of which are: the effective beam width model, and the equivalent frame model.

3.3.1 Effective Beam Width Model

The effective beam width model (EBWM) is based on an equal rotation concept, such that the rotation of the column in the original slab-column subassembly is equal to the rotation of the column in the equivalent beam-column subassembly (see Figure 3-8). The effective beam width is conventionally estimated using a factor α, such that: $L' = \alpha L_2$.

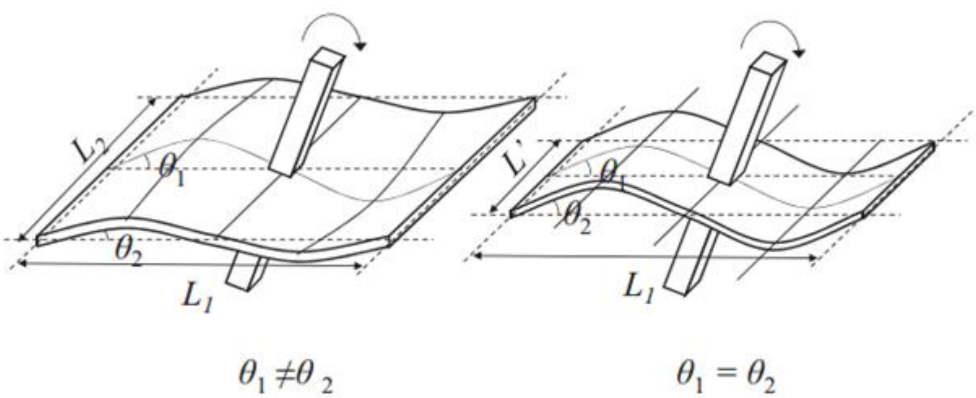

[a] [b]

Figure 3-8: Effective Beam Width Model: [a] Original Slab; [b] Effective Beam Model (Choi and Kim, 2015)

According to Hwang and Moehle (2000b), the effective width factor has been found to be mainly dependent on the span of the slab (l_1), as well as the column's dimension in the direction of the applied lateral load (c_1). Since proposing the EBWM by Pecknold (1975), many researchers have proposed different equations to estimate α (see Table 3-1). The effect of cracking due to gravity loading and seismic drifts is accounted for using a β factor (see Table 3-2), resulting in an effective slab width = $\alpha\beta.l_2$, where $l_2 =$ the full slab width.

Table 3-1: Estimation of the Effective Width Factor for Flat Slabs

Source	Proposed Equations
Banchick (1987)	$\alpha = \left(5\frac{c_1}{l_2} + \frac{1}{4}\frac{l_1}{l_2}\right)\frac{1}{1-v^2}$ [for interior connections] $\alpha = \left(3\frac{c_1}{l_2} + \frac{1}{8}\frac{l_1}{l_2}\right)\frac{1}{1-v^2}$ [for exterior connections]
Luo et al. (1995a; 1995b)	$\alpha = \dfrac{1.02\left(\frac{c_1}{l_2}\right)}{0.05 + 0.002\left(\frac{l_1}{l_2}\right)^4 - 2\left(\frac{c_1}{l_1}\right)^3 - 2.8\left(\frac{c_1}{l_1}\right)^2 + 1.1\left(\frac{c_1}{l_1}\right)}$ [for interior connections]
Grossman (1997)	$\alpha l_2 = K_d\left[0.3l_1 + c_1\frac{l_2}{l_1} + \frac{(c_2 - c_1)}{2}\right]\left(\frac{d}{0.9h}\right)K_{FP}$ With limits: $0.2K_dK_{FP}l_2 \le \alpha l_2 \le 0.5K_dK_{FP}l_2$ K_{FP} = 1.0 [interior]; 0.8 [edge]; 0.6 [corner]. K_d = 2.0 [for new structures]; 1.5 [for older structures].
Hwang and Moehle (2000b)	$\alpha l_2 = c_1 + \frac{1}{6}l_1$ [for exterior connections loaded parallel to the edge] $\alpha l_2 = 2c_1 + \frac{1}{3}l_1$ [for other connections]

Kang et al. (2009)	$\alpha = 0.75$ [for reinforced concrete connections] $\alpha = 0.70$ [for post-tensioned concrete connections] ▪ Average measured factors from shake table tests.
Youssef et al. (2014)	$\alpha = 10^{-16} R_a R_d \left(308 l_1^{\;2} - 2338 l_1 + 8415\right)\left(560 l_2^{\;2} - 7716 l_2 + 31235\right)$ $R_a = 3\left(\frac{P}{P_1}\right)^2 - 209\left(\frac{P}{P_1}\right) + 4764$ $R_a = 1761 D^2 - 8676 D + 13043$ ▪ The model is based on Grillage Analysis. ▪ P/P_1 represents nominal ratio of axial load to that of column. ▪ $D =$ Inter-storey drift ratio. l_1 and l_2 are in meters.

Table 3-2: Estimation of the Cracked Stiffness Factor for Flat Slabs

Source	Proposed Equations
Vanderbilt and Corley (1983); Moehle and Diebold (1985); Pan et al. (1988)	$\beta = \frac{1}{3}$
Luo et al. (1994; 1995a; 1995b)	$\chi = 1 - 0.4 \frac{V_g}{4A_c\sqrt{f'_c}} \equiv \beta$ ▪ f'_c = compressive strength of concrete in psi.
Hwang and Moehle (2000b)	$\beta = 5\frac{c}{l_1} - 0.1\left(\frac{LL}{40} - 1\right) \geq \frac{1}{3}$ ▪ LL = Service live load in unit of lb/ft^2.
Kang et al. (2009)	$\beta = 1/3$ [for reinforced concrete connections] $\beta = 2/3$ [for post-tensioned concrete connections] ▪ Average measured factors from shake table tests.
Han et al. (2009)	$\beta = 0.4 + 0.32\left[\left(\frac{M_a}{M_{cr}}\right)^{-0.5} - \left(\frac{M_a}{M_{cr}}\right)^{0.5}\right]$ [for interior connections] $\beta = 0.21 + 0.14\left[\left(\frac{M_a}{M_{cr}}\right)^{-0.5} - \left(\frac{M_a}{M_{cr}}\right)^{0.5}\right]$ [for exterior connections]

3.3.2 Equivalent Frame Model

The equivalent frame model (EFM) was first proposed by Corley et al. (1961), and was later adopted by early editions of both CSA A23.3 and ACI 318 as a gravity analysis method for two-way flat slabs. In this model, flat slabs are theoretically represented by a combination of flexural, torsional, and rigid elements as illustrated in Figure 3-9. Similar to the slab-beam elements in the EBWM, an effective width factor and a cracking factor are used to determine the width of the elastic flexural elements. In addition, at each slab-column joint, a portion of the slab with a width equal to the side face of the column is assumed to act as a torsional element.

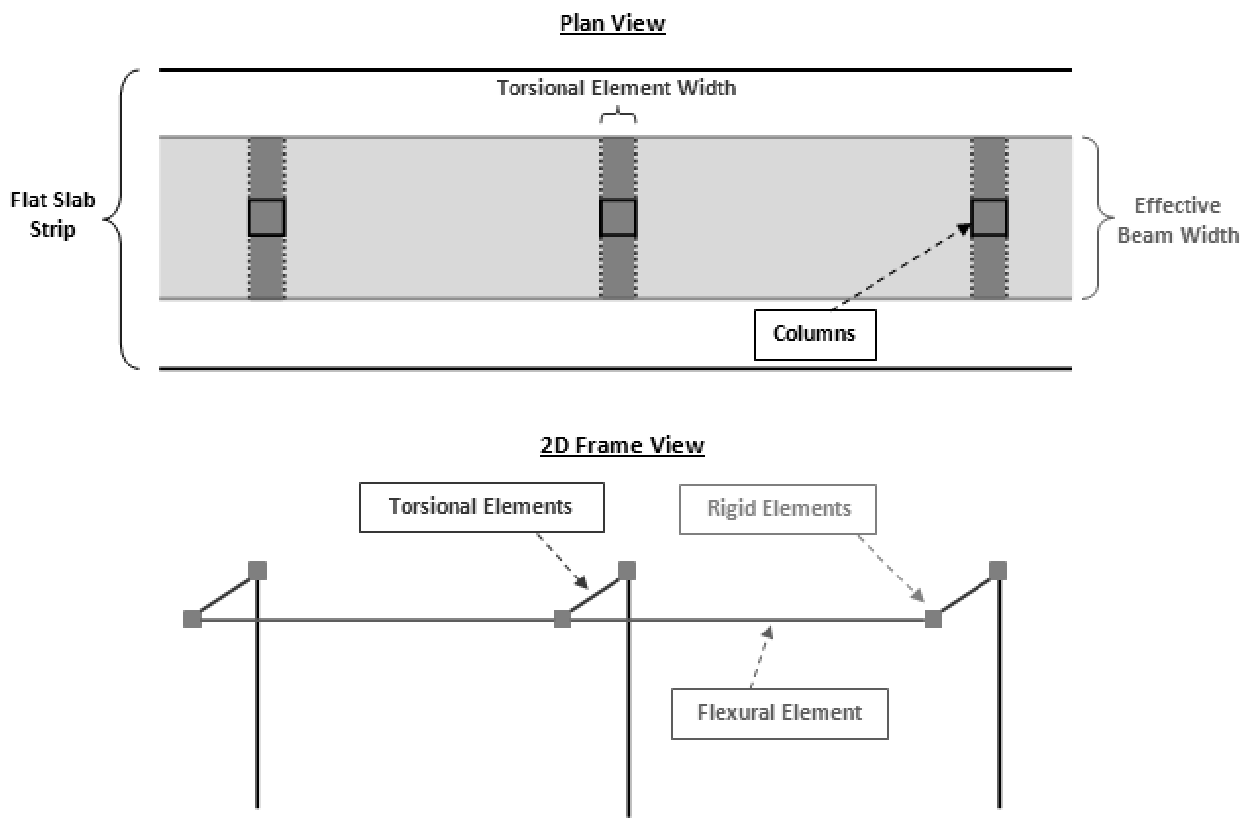

Figure 3-9: Illustration of the Equivalent Frame Model

In the EFM, an equivalent column is assumed for the 2-dimensional frame. The flexibility of the equivalent column is calculated based on flexibility contributions from the actual columns above and below the FSC connection, the flexural elements on both sides of the connection, and the torsional elements at the joint. Both CSA A23.3 (2014) and ACI 318 (2014) adopt the same equations developed by Jirsa et al. (1963) and Corley and Jirsa (1970) from 3-dimensional analytical studies.

<u>CSA</u> Clause 13.8.2.8; Clause 13.8.2.9 <u>ACI</u> Clause R8.11.5	$\frac{1}{K_{ec}} = \frac{1}{\sum K_c} + \frac{1}{K_t}$ $K_t = \sum \frac{9E_cC}{l_t\left(1-\frac{c_2}{l_t}\right)^3}$; where: $C = \sum\left(1-0.63\frac{x}{y}\right)\frac{x^3y}{3}$ ▪ $K_c =$ flexural stiffness of the column(s). ▪ $K_c =$ stiffness of the torsional element. ▪ $E_c =$ the concrete's modulus of elasticity. ▪ $x =$ the slab thickness, and $y =$ the column's side dimension. ▪ $c_2 =$ size of the equivalent rectangular column. ▪ $l_t =$ length of the torsional member.

For gravity design purposes, only relative stiffness values of the elements are required. However, for lateral analysis, the absolute stiffness values are necessary to obtain correct lateral displacements and internal forces. Thus, Hwang and Moehle (2000b) proposed the two following modifications to Corley and Jirsa's model:

- The length of the torsional element should be taken equal to l_1.

- The stiffness reduction factor used to account for cracking should be applied to the torsional elements only, and not to the flexural elements.

3.3.3 Comparison between the EBWM and the EFM

A study was conducted by Hwang and Moehle (2000b) to compare the analytical predications obtained using the two RCFS stiffness models to actual experimental results on a multi-bay FSC assembly. Figure 3-10 shows the comparison results, indicating that both approaches can provide acceptable estimates of the elastic lateral stiffness of the RCFS system. Therefore, the EBWM is adopted in the proposed nonlinear modeling technique presented in *Chapter 4*, due to its simplicity to implement in large numerical models.

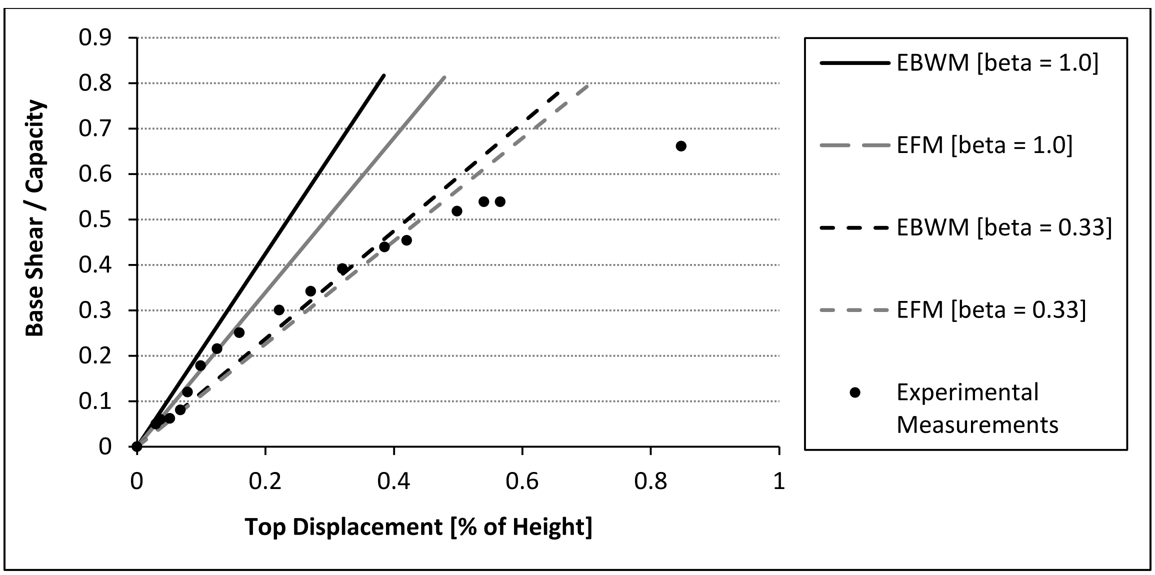

Figure 3-10: Comparison between the Effective Beam Width Model and the Equivalent Frame Model (Regenerated from a publication by Hwang and Moehle, 2000b)

3.4 Drift-Induced Punching Shear

As discussed in Section 2.3, punching shear failure may occur when a FSC connection is subjected to a combination of a gravity load and lateral drifts, even if the nominal shear stress capacity is not exceeded. This phenomenon has been investigated by some researchers, such as Pan and Moehle (1989), Megally and Ghali (1994), Hueste and Wight (1999), Kang and Wallace (2006), and Hueste et al. (2007; 2009).

Kang and Wallace (2006) provided an explanation to this phenomenon analogous to Sezen's (2002) shear strength degradation model of RC columns. The punching shear capacity of a FSC connection degrades with increasing lateral drifts. Consequently, when the shear demand exceeded the reduced capacity of the connection, punching shear failure occurs (see Figure 3-11).

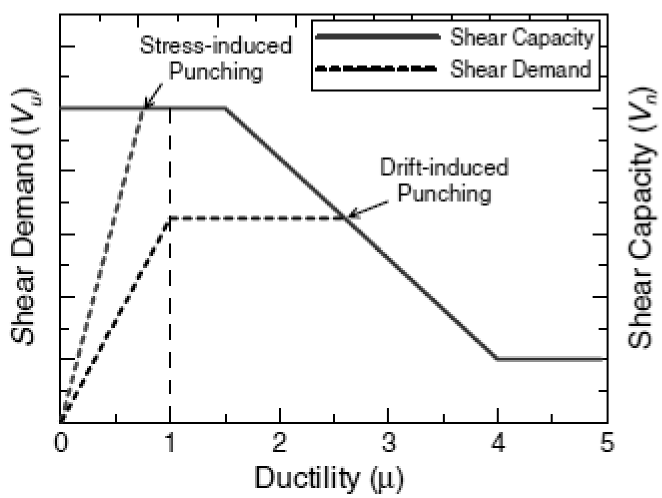

Figure 3-11: Relationship between Ductility and Shear Capacity / Demand (Kang and Wallace, 2006)

By compiling data from various experimental studies, researchers have related the deformation capacity of FSC connections to the applied gravity shear ratio $\left(V_g / \phi V_c\right)$. Figure

3-12 shows experimental test results of 26 specimens with shear reinforcement. It should be noted that the gravity shear ratios were calculated based on actual material properties, i.e. $\phi = 1.0$.

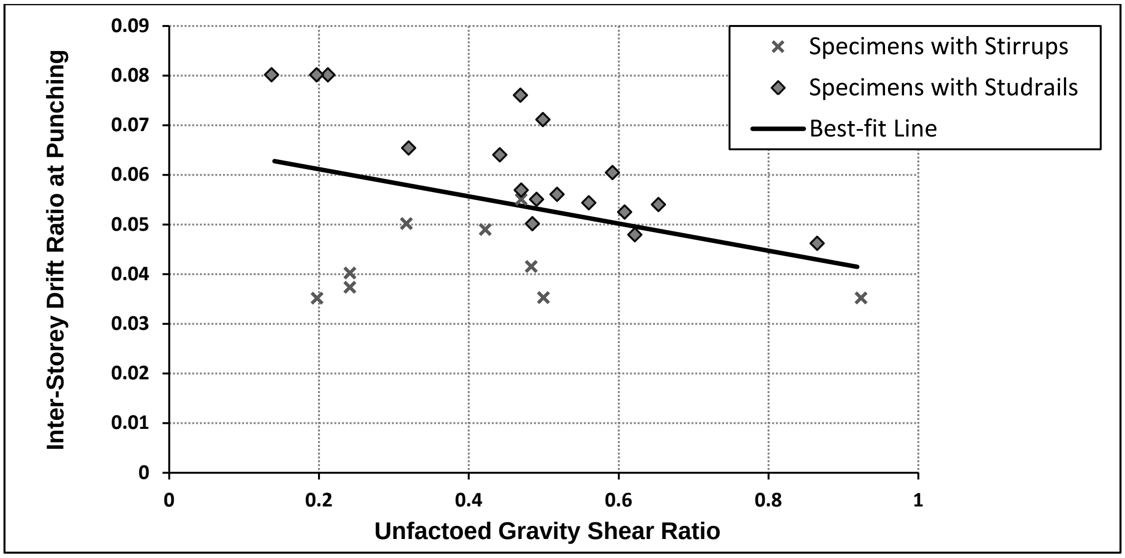

Figure 3-12: Inter-Storey Drift Ratio at Punching vs. Gravity Shear Ratio (Regenerated from a publication by Kang and Wallace, 2006)

In *Chapter 4*, data from new experimental studies are added to the data collected by Kang and Wallace (2006). The maximum inter-storey drift limit proposed for the nonlinear modeling technique is based on these compiled data.

CSA A23.3 (2014) and ACI 318 (2014) adopt the same trend for seismic design guidelines. For FSC connections that are not considered part of the SFRS, the seismic provisions in both codes require shear reinforcement to be provided when the combination of the inter-storey drift ratio and the factored gravity shear ratio at a FSC connection is above certain limits, as follows:

<u>CSA</u> Clause 21.11.4	Shear reinforcement is required if the direct shear stress from seismic load combinations exceeds $R_E.v_r$, such that: ▪ $R_E = \left(\frac{0.005}{\delta_i}\right)^{0.85} \leq 1.0$ ▪ $\delta_i =$ inter-storey drift ratio ▪ Clause 21.11.4.2 sets the minimum requirements for seismic shear reinforcement design.
<u>ACI</u> Clause 18.14.5.1	Shear reinforcement is required if: $\Delta_x / h_{sx} \geq 0.035 - \frac{1}{20}\left(v_{ug} / \phi v_c\right)$, where: ▪ $\Delta_x / h_{sx} =$ inter-storey drift ratio. ▪ $v_{ug} / \phi v_c =$ factored gravity shear ratio. ▪ No seismic shear reinforcement required if $\Delta_x / h_{sx} \leq 0.005$. ▪ Minimum requirements for shear reinforcement are provided by Clauses 8.7.6 and 8.7.7.

Figure 3-13 shows a graphical comparison between the limits enforced by both design codes.

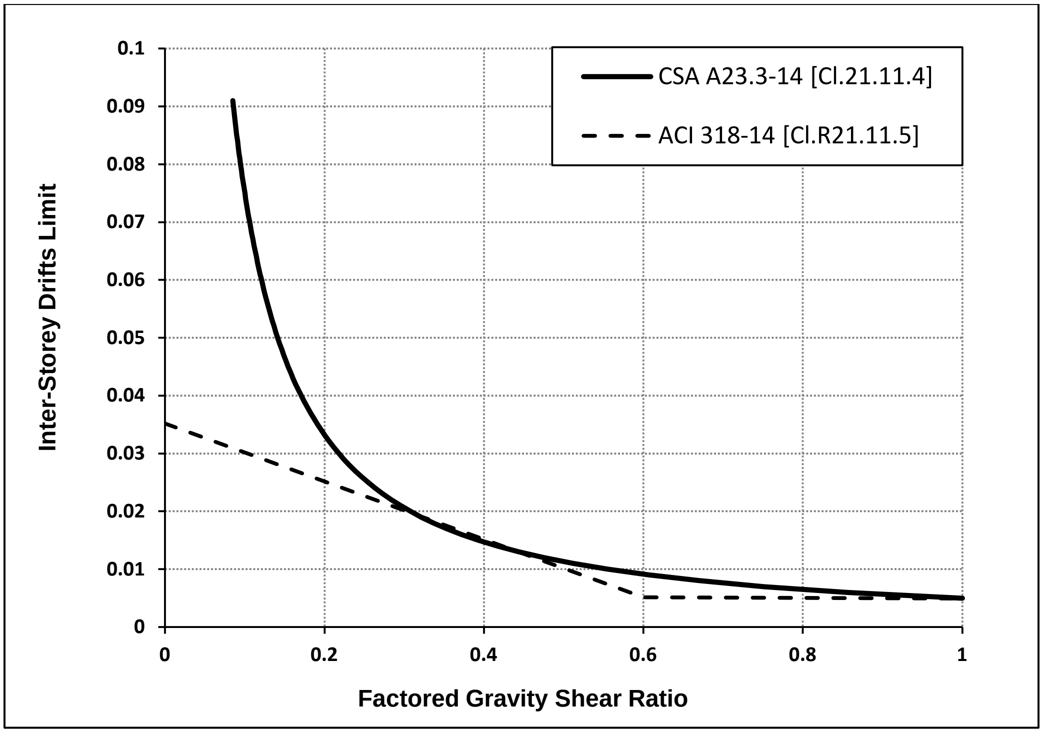

Figure 3-13: Comparison between the Seismic Shear Reinforcement Provisions of CSA A23.3 (2014) and ACI 318 (2014)

Chapter 4: Proposed Nonlinear Modeling Technique

4.1 Overview

Based on the discussions provided in *Chapters 2 and 3* on the behaviour of FSC connections and the related analytical models, this chapter presents a new lumped-plasticity model to simulate the nonlinear dynamic response of FSC connections with shear reinforcement. Due to the limitations of the existing nonlinear models (discussed in *Chapter 1*), the presented model was developed to capture the hysteretic response of ductile FSC connections, and detect potential failures during time-history analyses due to all possible modes of failure. The proposed model is verified with actual experimental data (by Park et al., 2011) on specimens with varying material properties and different types of shear reinforcement.

4.2 Subassembly Modeling

In accordance with the eccentric shear stress approach adopted by ACI 318 (2014) and CSA A23.3 (2014), when a FSC connection is subjected to an unbalanced moment (M_u), a portion of the moment $\left(\gamma_v M_u\right)$ resisted by the vertical eccentric shear stress, while the other portion $\left(\gamma_f M_u\right)$ is resisted by the slab's flexural reinforcement (see Figure 4-1). In order to account for both modes of failure, two types of plastic hinges are used: shear hinges, and rotational hinges. Figure 4-2 shows the proposed modeling technique of an interior FSC subassembly. Due to the lack of experimental data available in 3 dimensions, the model is only calibrated in 2 dimensions. The 3 dimensional response of the RCFS is therefore assumed to be modeled using two uncoupled lumped plastic hinge models in orthogonal directions. Once additional experimental data are available, the coupled response of the FSC connections with shear reinforcement in 3 dimensions can be accounted for.

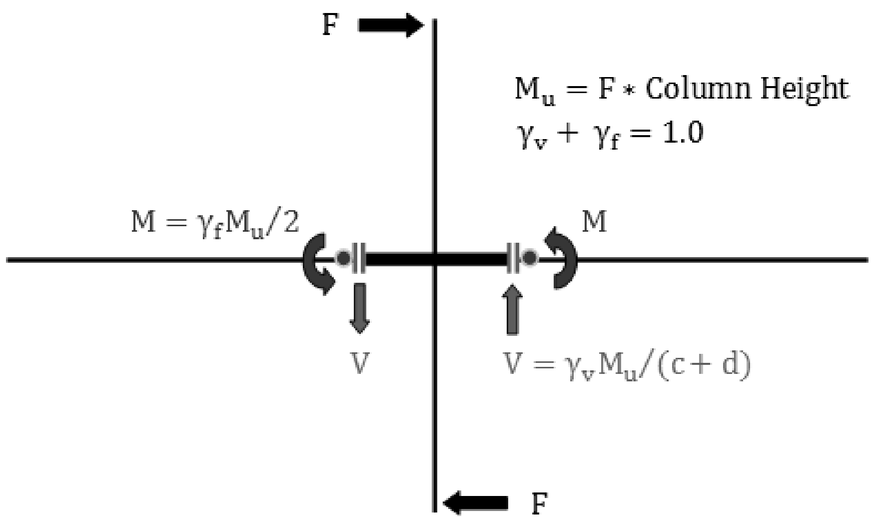

Figure 4-1: Equilibrium in the FSC System When Subjected to Unbalanced Moments

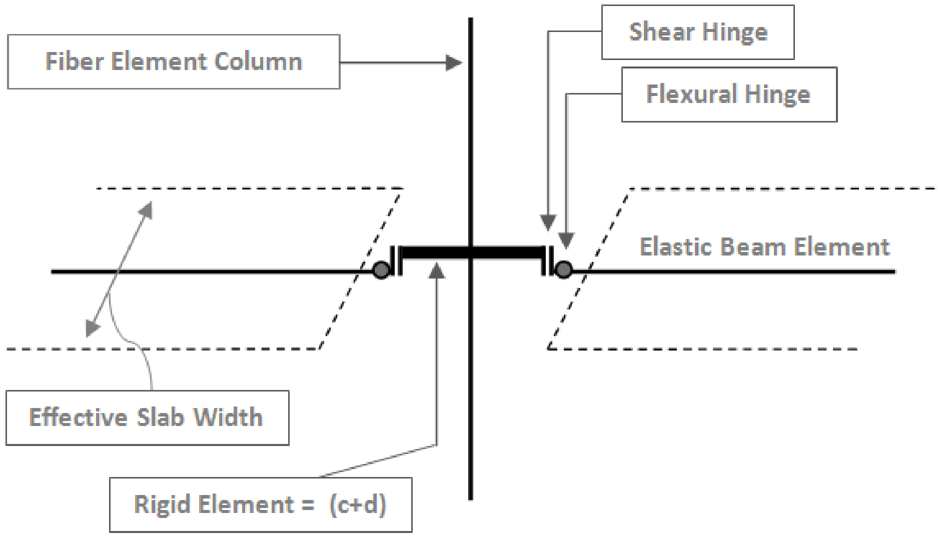

Figure 4-2: FSC Subassembly Modeling

4.3 Lateral Stiffness

The effective beam width model proposed by Hwang and Moehle (2000b) is adopted in the proposed modeling technique. The model introduces an α factor to estimate the reduced elastic lateral stiffness of RCFS. The stiffness reduction due to cracking is also accounted for by using a β_{cr} factor, resulting in an effective slab width = $\alpha\beta_{cr}.l_2$, where $l_2 =$ the full slab width. The reduction factors are estimated using *Equations 4.1 and 4.2*, which are based on extensive experimental and analytical studies:

$$\alpha l_2 = 2c_1 + \frac{1}{3}l_1 \geq \frac{1}{3} \qquad \textbf{Equation 4.1}$$

$$\beta_{cr} = 4\frac{c_1}{l_1} \geq \frac{1}{3} \qquad \textbf{Equation 4.2}$$

where: $l_1 =$ center-to-center span in the longitudinal direction; $l_2 =$ center-to-center span in the transverse direction; $c_1 =$ rectangular column cross-sectional dimension parallel to dimension l_1.

4.4 Shear Hinge Properties

The resultant shear stress at a FSC due to a gravity load and an unbalanced moment is expressed by *Equation 4.3*:

$$v_u = \frac{V_u}{b_o d} + \gamma_v \frac{M_u e}{J} \qquad \textbf{Equation 4.3}$$

$$\gamma_v = 1 - \frac{1}{1 + \frac{2}{3}\sqrt{b_1/b_2}} \qquad \textbf{Equation 4.4}$$

where: $V_u =$ factored gravity load applied within the tributary area of the connection; $b_o =$ perimeter of the critical section; $d =$ effective slab depth; $M_u =$ applied unbalanced moment; $e =$ distance from center of column to critical section face; $\gamma_v =$ the fraction of unbalanced moment transferred by eccentricity of shear *(Equation 4)*; $J =$ property of the critical section analogous to polar moment of inertia; $b_1 =$ dimension of the critical section parallel to the direction of the unbalanced moment; $b_2 =$ dimension of the critical section perpendicular to the direction of the unbalanced moment.

Hence, the unbalanced moment capacity could be calculated using the rearranged *Equation 4.5*:

$$M_{np} = \left(v_c + v_s - \frac{V_u}{b_o d} \right) \frac{J}{\gamma_v \left(\frac{c+d}{2} \right)}$$ **Equation 4.5**

where: $v_c =$ shear stress resistance provided by the concrete; $v_s =$ shear stress resistance provided by the shear reinforcement; $c =$ column cross-sectional dimension along the direction of the unbalanced moment (or lateral drift).

Figure 4-4 shows the force-deformation relationship of the shear hinge. V_p represents the shear capacity which corresponds to an ultimate plastic shear deformation of Δ_p. The force drops to zero once the ultimate deformation is reached, indicating that shear failure has occurred. The shear hinge properties can be estimated using *Equations 4.6 and 4.7*, respectively.

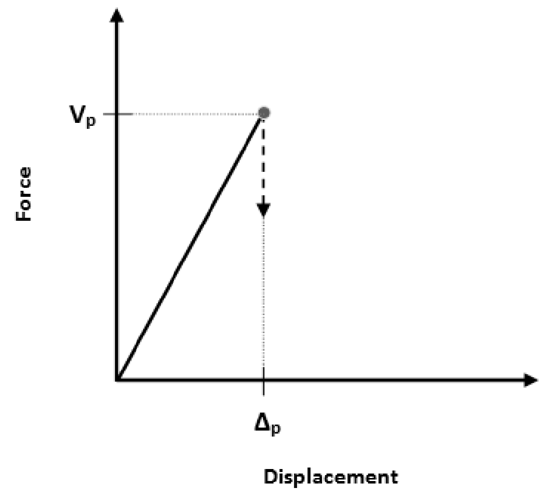

Figure 4-3: Backbone of Shear Hinge

$$V_p = \left(\frac{M_{np}}{c+d} \right)$$ **Equation 4.6**

$$\Delta_p = \frac{\theta_p}{2}(c+d)$$ **Equation 4.7**

where: θ_p is the critical rotation at which punching shear failure is expected to occur (see Figure 2). It should be noted that columns of the FSC experimental subassemblies are usually stiff compared to the rotational stiffness of the slab. Hence, the maximum rotations of experimental FSC subassemblies are assumed to be equal to the maximum inter-storey drift ratios.

The critical rotation limit proposed on Figure 4-4 is based on a compilation of data from experimental tests of FSC connections with shear multiple types of shear reinforcement. The critical rotation was assumed to be equal to the recorded inter-storey drift at which punching shear failure is detected. This is because in such tests, the FSC specimens usually contain columns that are rigid compared to the rotational stiffness of flat slabs.

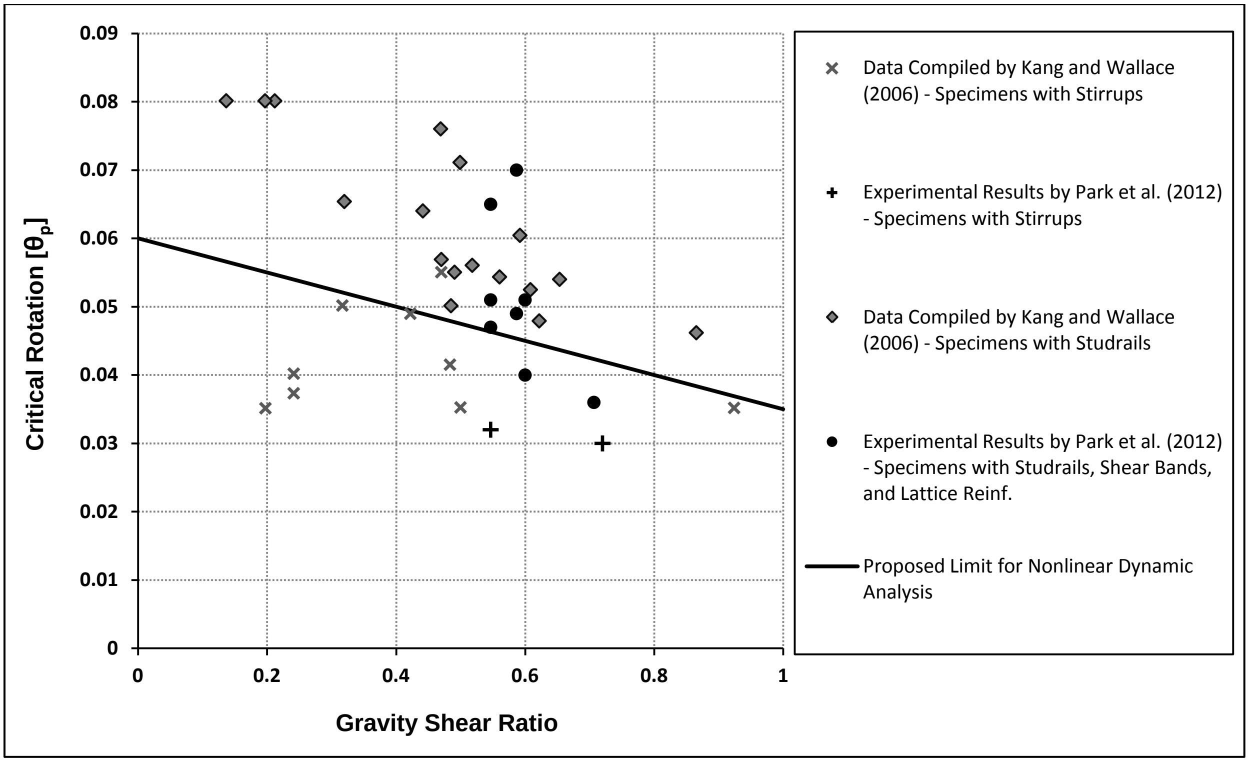

Figure 4-4: Critical Rotation for Punching Shear Capacity Calculations

4.5 Flexural Hinge Properties

In addition to the shear hinges, parallel flexural hinges are assigned to the FSC connection to simulate the flexural response of the connection. The flexural capacity of the connection can be determined from cross-sectional analysis of a slab with a flexure-transfer width of $c_2 + 3h$, where $c_2 =$ rectangular column cross-sectional dimension perpendicular to the direction of the applied load, $h =$ thickness of slab. Figure 4-5a shows a typical moment-curvature response of the FSC connection obtained from fiber analysis of reinforced concrete section.

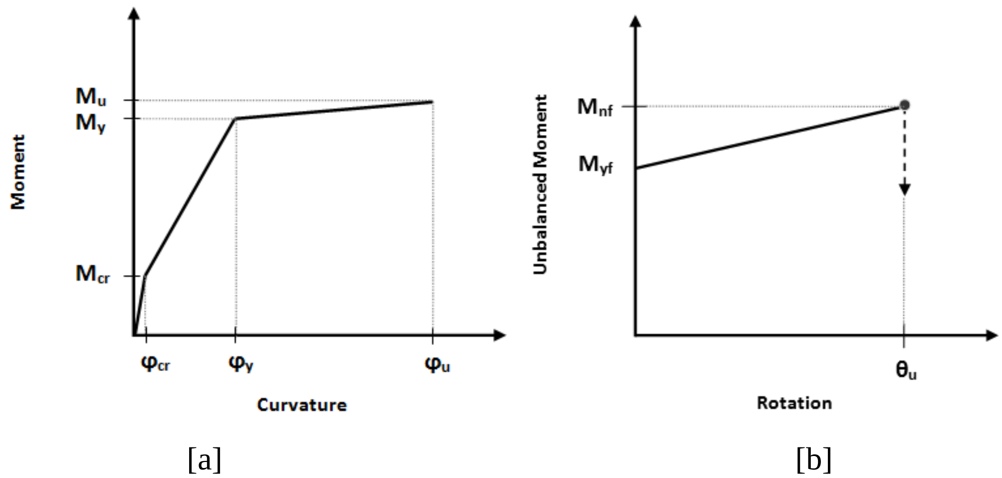

Figure 4-5: [a] Typical Moment-Curvature Relationship of a Bending Slab-Beam; [b] Backbone of Flexural Hinge

Using a plastic hinge length equal to the effective depth of the slab (d), the moment-rotational backbone of the flexural hinge (Figure 4-5b) can be estimated using *Equations 4.8 to 4.10*. Once the ultimate deformation (θ_u) is reached, the moment capacity will drop to zero, indicating that flexural capacity is exhausted.

$$M_{yf} = M_y \qquad \textbf{Equation 4.8}$$

$$M_{nf} = M_u \qquad \textbf{Equation 4.9}$$

$$\theta_u = l_p\left(\varphi_u - \varphi_y\right) \qquad \textbf{Equation 4.10}$$

where: l_p = the plastic hinge length ≈ d; ; φ_y = yield curvature of the cross section (see Figure 4-5a); φ_u = ultimate curvature of the cross section $= \varepsilon_u / c$, such that ε_u = ultimate strain of concrete at maximum stress and c = depth of neutral axis.

4.6 Hysteresis Rules for the Flexural Hinges

Figure 4-6 shows the proposed analytical model to simulate the force-deformation flexural response of FSC connections. The horizontal axis represents the joint rotation, and the vertical axis represents the moment at the rotational hinge of the connection. The proposed hysteresis model is defined using the backbone curve as illustrated in Figure 4-5b. It should be noted that response in positive direction can be different than the negative direction, i.e. M_{yf}^{+} may not be equal to M_{yf}^{-}, and similarly M_{nf}^{+} may not be equal to M_{nf}^{-}. This is because the top and bottom longitudinal steel reinforcement ratios within the flexure-transfer width are usually different.

The dotted lines in Figure 4-6 illustrate the hysteresis rules that the moment-rotational response follows. When a the plastic hinge starts to deform either towards the positive or the negative direction, the response follows an initial elastic stiffness of K_0. The value of the elastic stiffness (K_0) need not be defined, since the elastic behaviour of the RCFS is captured by the elastic beam element (with a width of $\alpha\beta_{cr}.l_2$) in the FSC subassembly. The elastic behaviour is bounded by the backbone curve defined by M_{yf} and M_{nf}.

Once the hinge's deformation reaches the yield limit, it will follow the backbone curve, and the plastic hysteretic rules are activated. The point of maximum rotation and moment on both the positive and negative sides is recorded, and it will be updated whenever exceeded. If the deformation path changes direction, the moment-rotational response will follow the initial elastic stiffness, K_0 until the virtual plateau defined by M_0^{+} or M_0^{-} in the positive and negative directions, respectively, is reached. Once the curve reaches the virtual plateau, the moment-rotational response is diverted towards M_0^- and M_0^+ in the positive and negative directions, respectively.

If the deformation path passes the pivot points $(0, M_0^-)$ or $(0, M_0^+)$, the moment-rotational response goes towards the point with the maximum recorded deformation and force from previous cycles, taking into account cyclic degradation using a slope discounting factor ρ. At any given moment of time, if the deformation reverses, it will follow the initial stiffness K_0 until the backbone curve on either side is reached.

For FSC connections with shear reinforcement, a suggested value for M_0 is 12% of the estimated M_{nf}. This ratio is based on calibration of 16 different experimental specimens, as shown in Figure 7. The same analytical calibrations suggest a ρ factor of 0.93 to 0.95 which represent stiffness degradation of 5 to 7% per cycle.

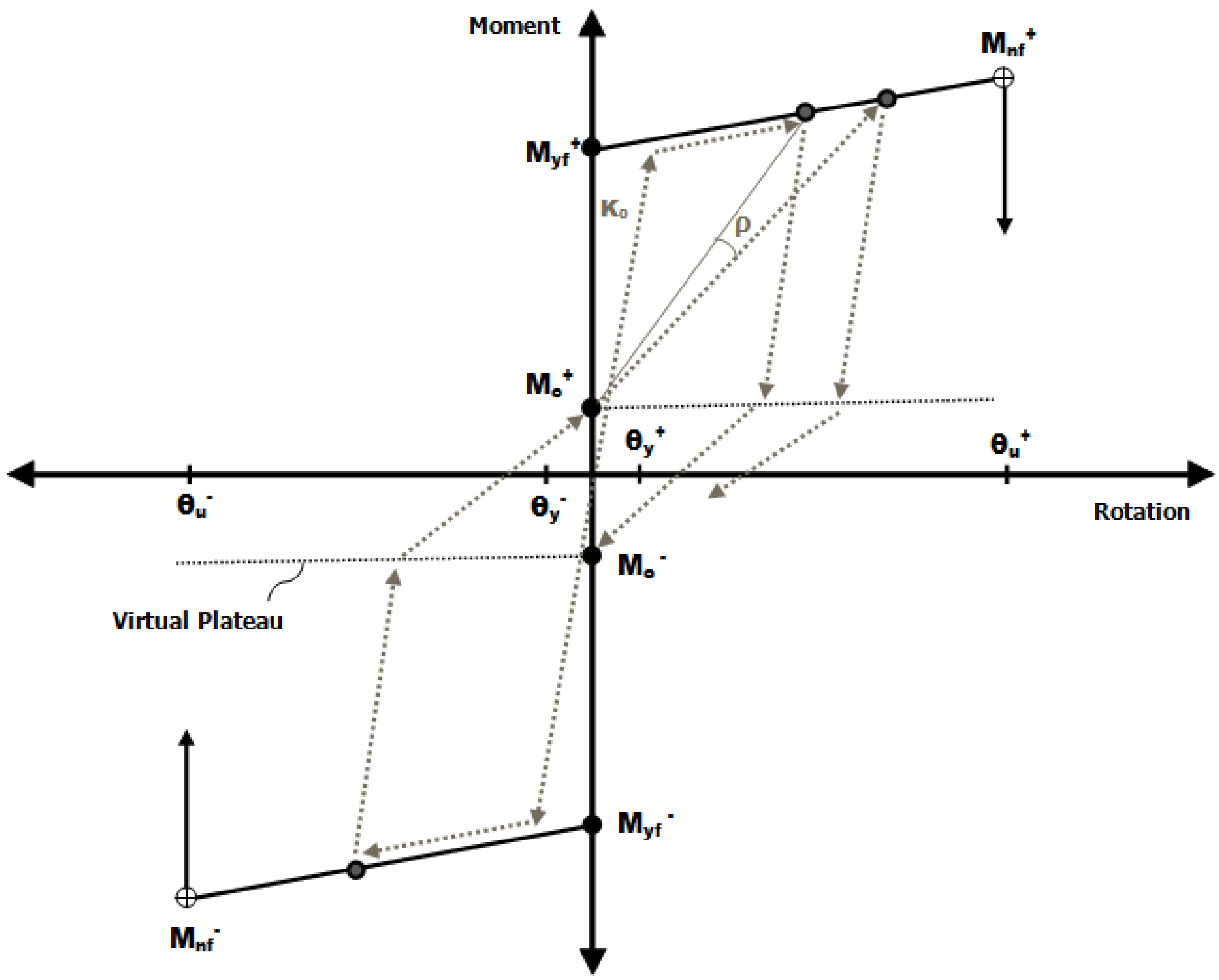

Figure 4-6: Proposed Hysteresis Model

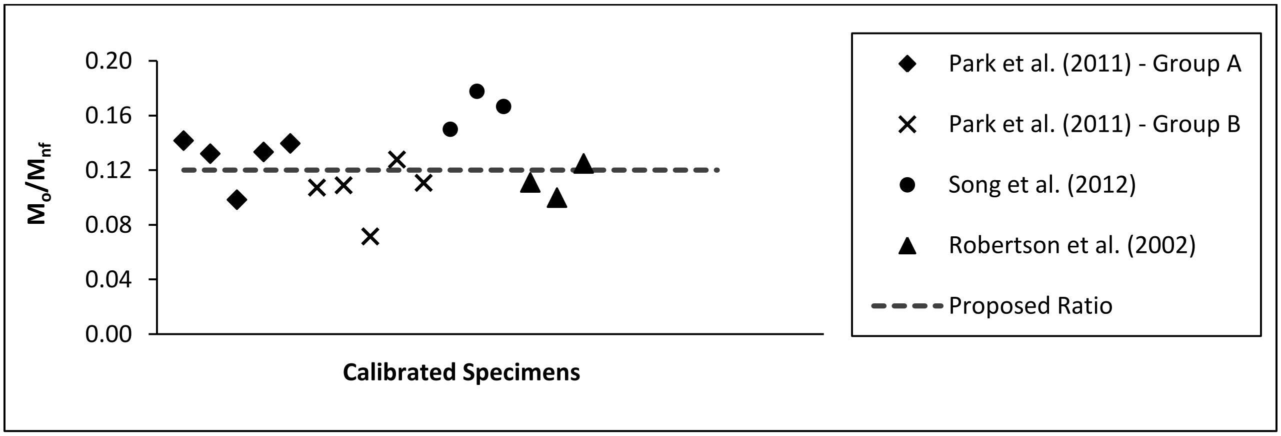

Figure 4-7: M_o to M_{nf} Ratio from Calibrations to Experimental Data

4.7 Verification of the Proposed Model

The proposed model has been verified against several experimental tests, one of which is an extensive experimental program conducted by Park et al. (2011). The study included twelve FSC connections with varying concrete strengths and multiple types of shear reinforcements which undergo cyclic pushover tests. Three of the specimens were used to compare the hysteresis response generated by the proposed numerical model. These 3 specimens were selected such that they vary in concrete strength, type of shear reinforcement, and the gravity shear ratio. Table 4-1 shows the details of the specimens verified. A comparison between the predicted modeling parameters and the experimental results is presented in Table 4-2.

Comparing the nominal capacities estimated numerically (M_{np} and M_{nf}), it is predicted that that specimens SB-A and SR-A will fail in punching shear, while in specimen LR-B1 longitudinal reinforcement yielding will occur prior punching shear.

Table 4-1: Verification Specimens (Park et al., 2011)

Specimen	f'_c (MPa)[1]	Type of Shear Reinforcement	v_u/v_c[2]	v_s/v_c[3]	Experimental Test Results	
					M_{exp} (kN.m)	Max. Drift Ratio
SB-A	22.5	Shear Bands	0.45	2.41	96.7	5.1 %
SR-A	22.5	Studrails	0.45	1.94	98.9	4.0 %
LR-B1	38.7	Lattice Reinforcement	0.41	1.54	129.1	4.7 %

[1]: Compressive strength of concrete.

[2]: Ratio between direct punching shear stress to punching shear strength of concrete ($v_c = \sqrt{f'_c}/3$) MPa.

[3]: Ratio between punching shear strength of the shear reinforcement to punching shear strength of concrete.

Table 4-2: Comparison between Experimental Results and Numerical Predictions

Specimen		Experimental Test Results		Numerical Predictions				$\frac{M_{exp}}{M_n}$
		M_{exp} (kN.m)	Maximum Drift	M_{np}	M_{nf}	M_n (kN.m)	Maximum Drift	
1	SB-A	96.7	0.051	108.3[1]	109.6	108.3	0.045	0.89
2	SR-A	98.9	0.040	108.3[1]	109.6	108.3	0.045	0.91
3	LR-B1	129.1	0.047	149.3	115.2[2]	115.2	0.046	1.12

[1]: Governing unbalanced moment capacity due to punching shear stress.

[2]: Governing unbalanced moment capacity due to flexure.

Figure 4-8, Figure 4-9, and Figure 4-10 show the comparison of the hysteresis for specimens SB-A, SR-A and LR-B1, respectively. The result shows that the proposed numerical model is capable of simulating the nonlinear response of the FSC connections.

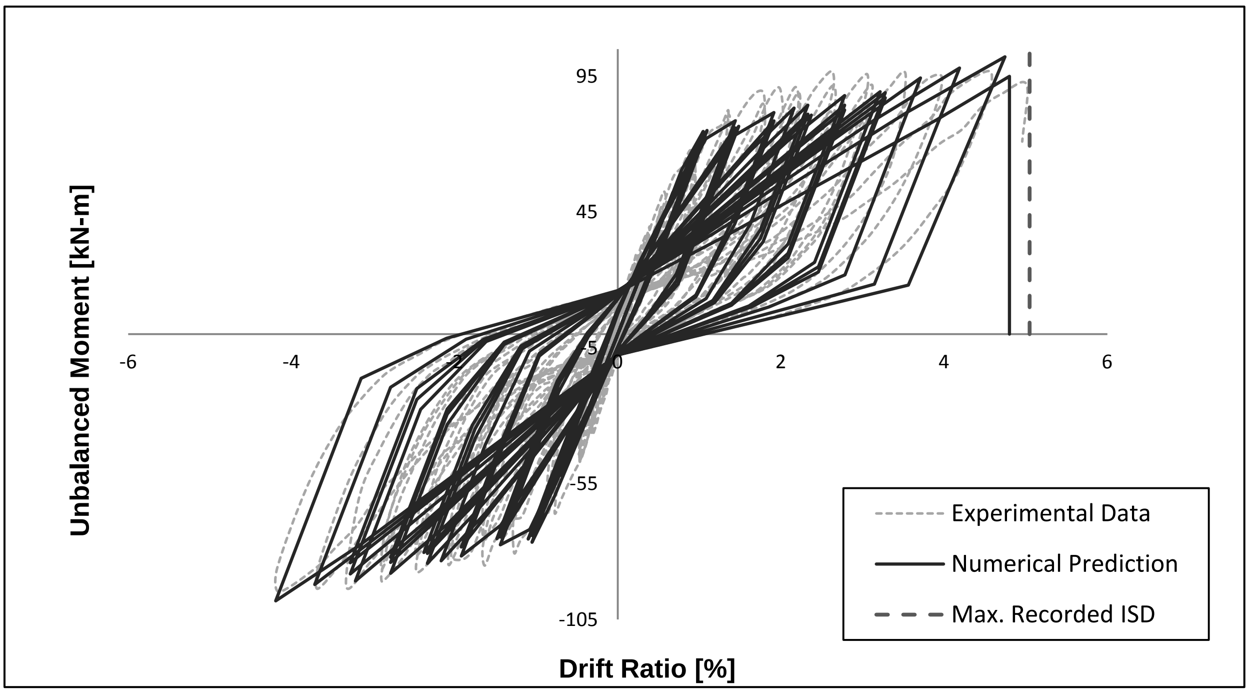

Figure 4-8: Comparison between the Experimental Response and the Numerical Prediction of Specimen #1

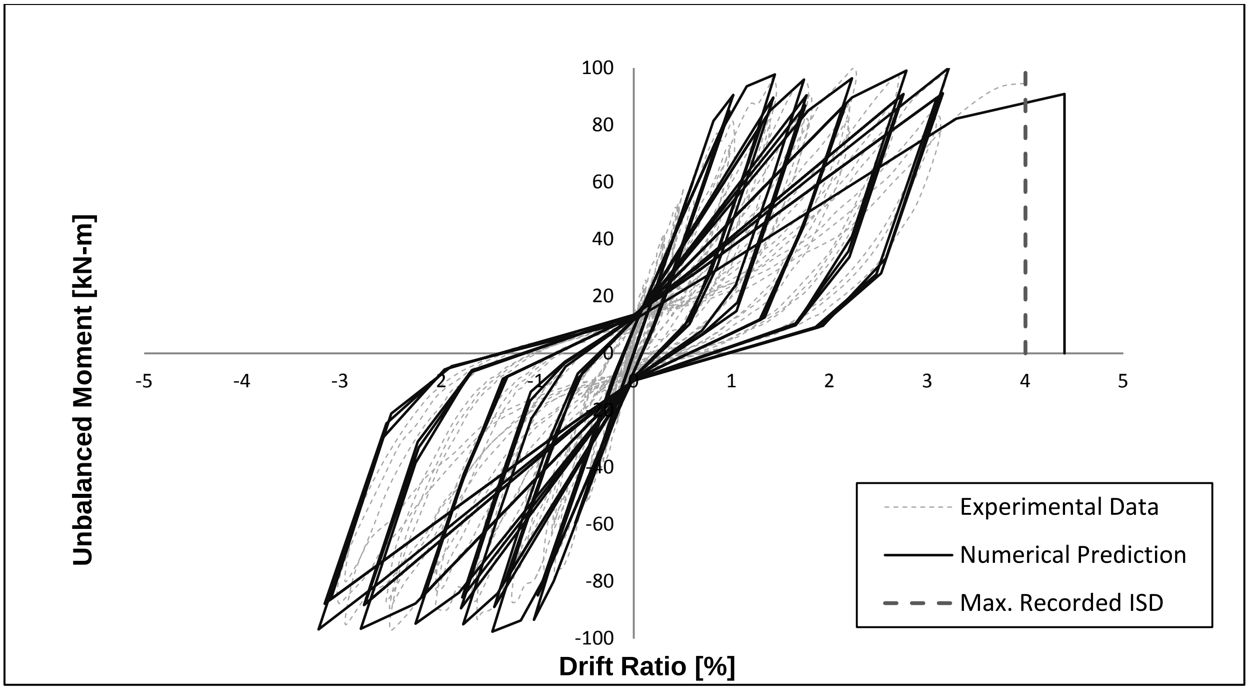

Figure 4-9: Comparison between the Experimental Response and the Numerical Prediction of Specimen #2

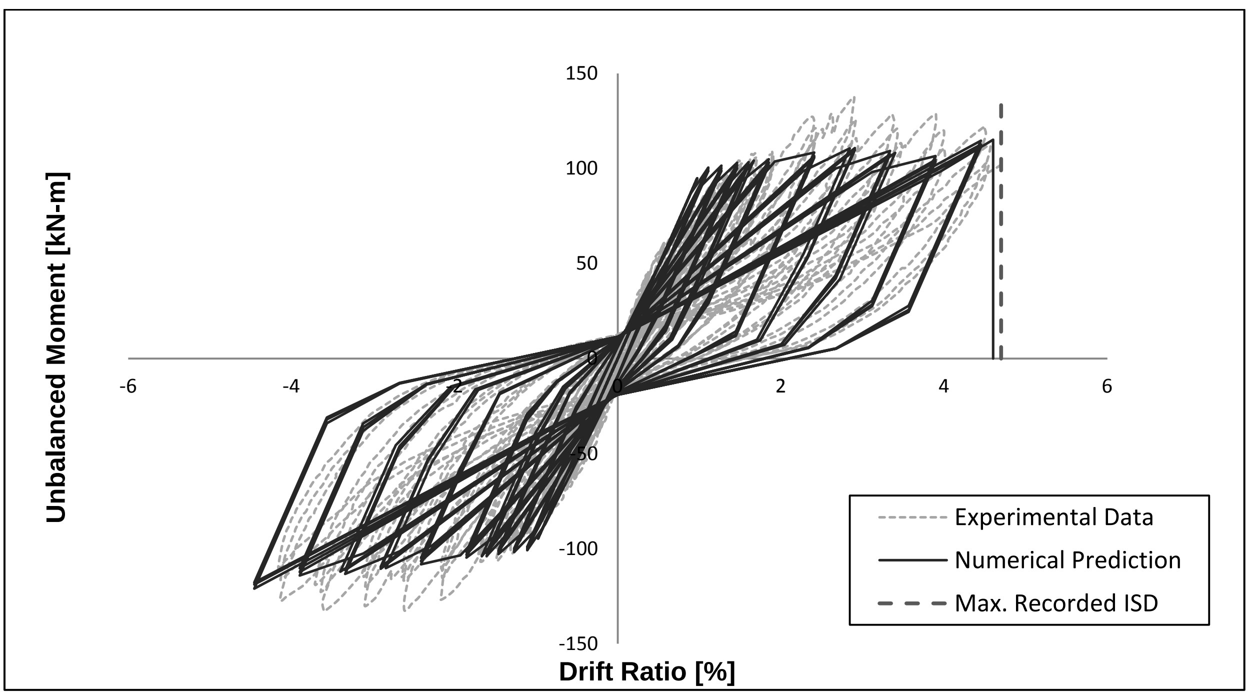

Figure 4-10: Comparison between the Experimental Response and the Numerical Prediction of Specimen #3

Chapter 5: Case Studies on a Typical Tall Building

5.1 Overview

In this chapter the effects of the seismic behaviour of RC flat slabs on the global response of high-rise buildings are investigated. Two case studies were conducted on a typical 40-storey building located in Vancouver, Canada. Results from the first study show the significance of including the RCFS system in the analysis model for multiple reasons. The second study investigates the impact of different slab designs on the global nonlinear response of the structure.

5.2 Description of the Prototype Building

5.2.1 Structural System

A tall reinforced concrete shear wall building with flat-plate gravity framing was designed using a performance-based approach. The building consists of 40 stories in addition to 4 basement levels [137.5-meter high above ground level], with a footprint of 742.5 m^2 and 2320 m^2 for super-structure levels and basements levels, respectively. Figure 5-1 shows the typical layout of the super-structure floors. The core walls were proportioned for design-level ground motions so that the inelastic response would be restricted to flexural yielding of the wall at the base for the ductile walls [N-S direction], and flexural yielding at the base and the coupling beams over the height and for the coupled walls [E-W direction]. RCFS with headed shear reinforcement (shear studs) were used as a typical flooring system for all stories above ground level.

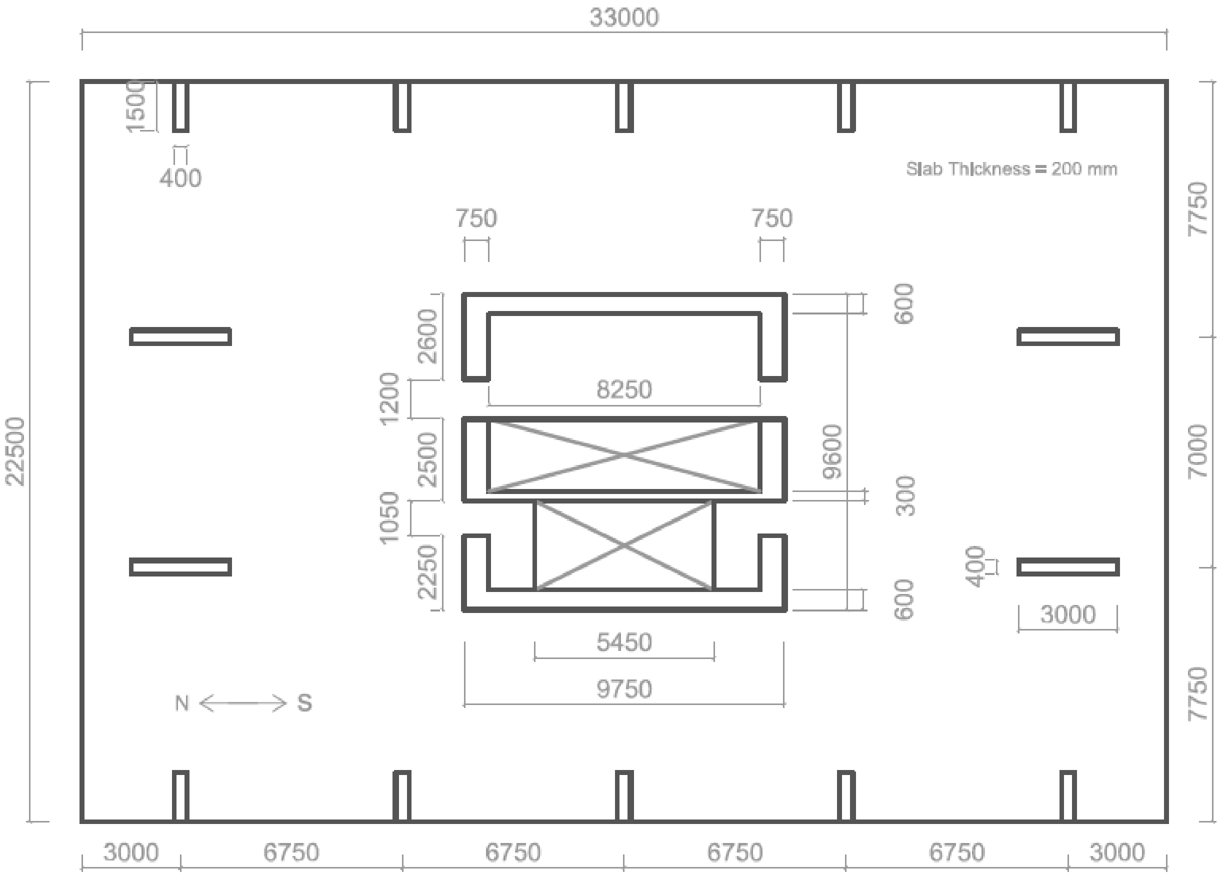

Figure 5-1: Typical Super-Structure Floor Plan

5.2.2 Gravity Loads and Lateral Demands

All the structural elements were designed in accordance with the Canadian concrete code: CSA A23.3 (2004, 2009), following standard procedures to estimate demands as prescribed by the National Building Code of Canada (NBCC, 2010). Table 5-1 summarizes the gravity loads used in all subsequent analysis of the prototype building.

Wind loads were calculated in accordance with the dynamic procedure of NBCC (2010). The reference velocity pressure corresponding to the 1 in 50 year probability of exceedance was assumed to be 0.45 kPa for downtown Vancouver. Exposure class B (rough terrain) was assumed.

Table 5-1: Gravity Load Values for Different Zones

Zone Category	SDL [kPa]	LL [kPa]
Residential Floors	1.44	1.92
Parking Areas	0.24	2.40
Stairs / Corridors	-	4.80
Roof	4.08	1.91

For seismic demands, the uniform hazard design spectral values for site class B (Figure 5-2) as per Clause 4.1.8.4(7) in NBCC (2010) are adopted.

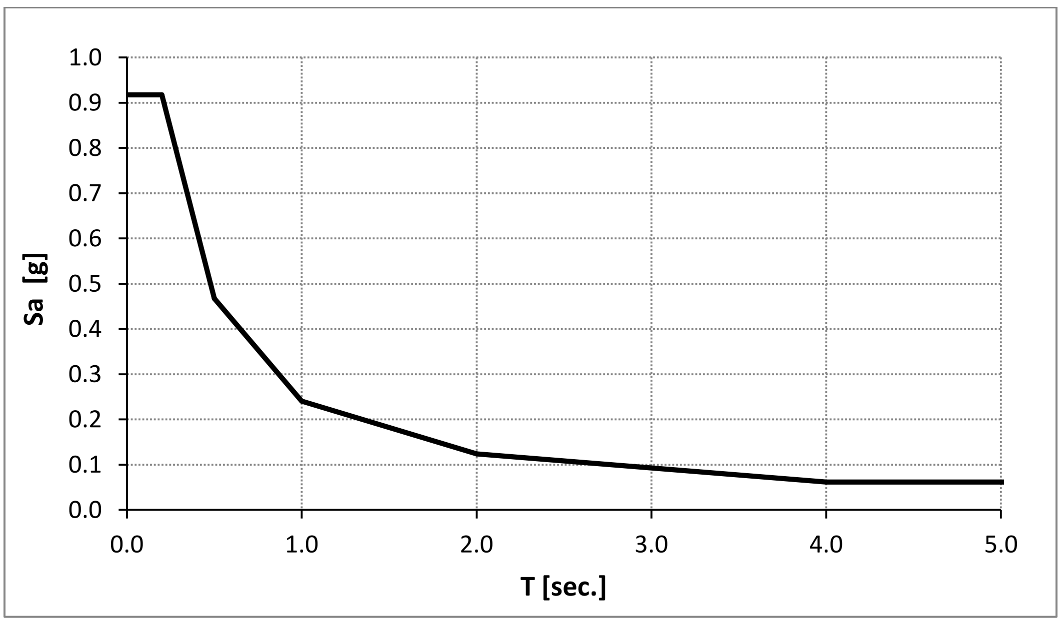

Figure 5-2: Uniform Hazard Spectrum for Vancouver, Site Class B (NBCC, 2010)

A design summary of the building is included in the appendix.

5.3 Nonlinear Modeling Procedure

5.3.1 Description of the Model

An analytical model was developed using OpenSees (PEER, 2015a). Expected gravity loads (1.0D + 0.25S) were applied to the model as point loads on the nodes. As stated in the modeling approach, the model is currently applicable in 2 dimensions due to the lack of experimental tests in 3 dimensions, hence only the response of the building in the North-South direction is presented. Rayleigh mass and stiffness proportional damping of 0.025 was assigned to the 1st and 3rd translational mode of vibration.

The RCFS-columns connections were modeled as using the lumped hinge modeling technique proposed in Chapter 4. Slab-wall connections were assumed to have the same properties of the opposite FSC connections. The core walls and the gravity columns were modeled using the displacement-based nonlinear beam column element with fiber sections. The base of the walls were fixed, while the base of the columns were pin supported. Figure 5-3 and Figure 5-4 illustrate the model developed in OpenSees.

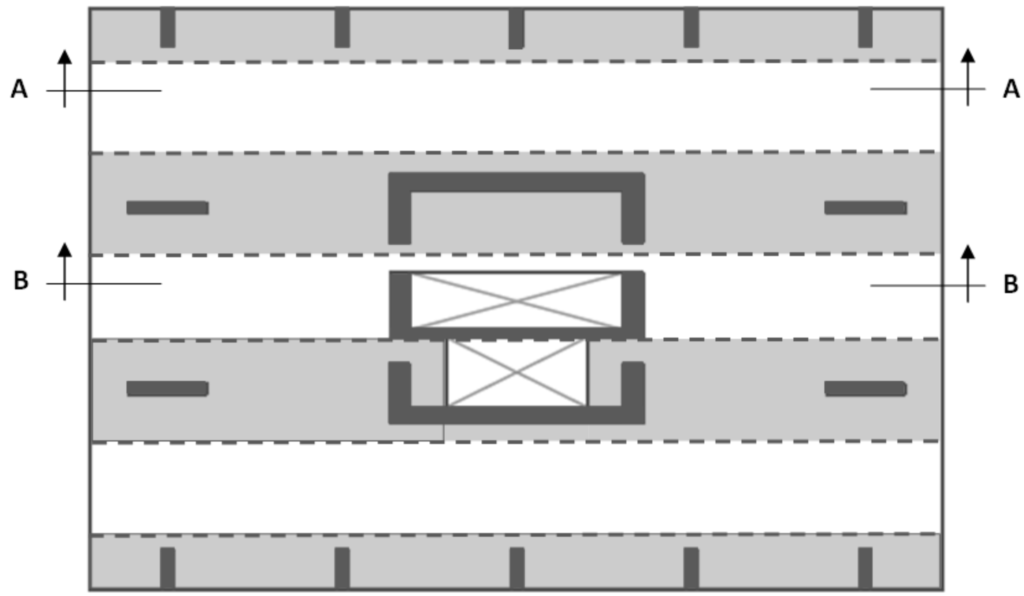

Figure 5-3: Plan View of the Equivalent Frames

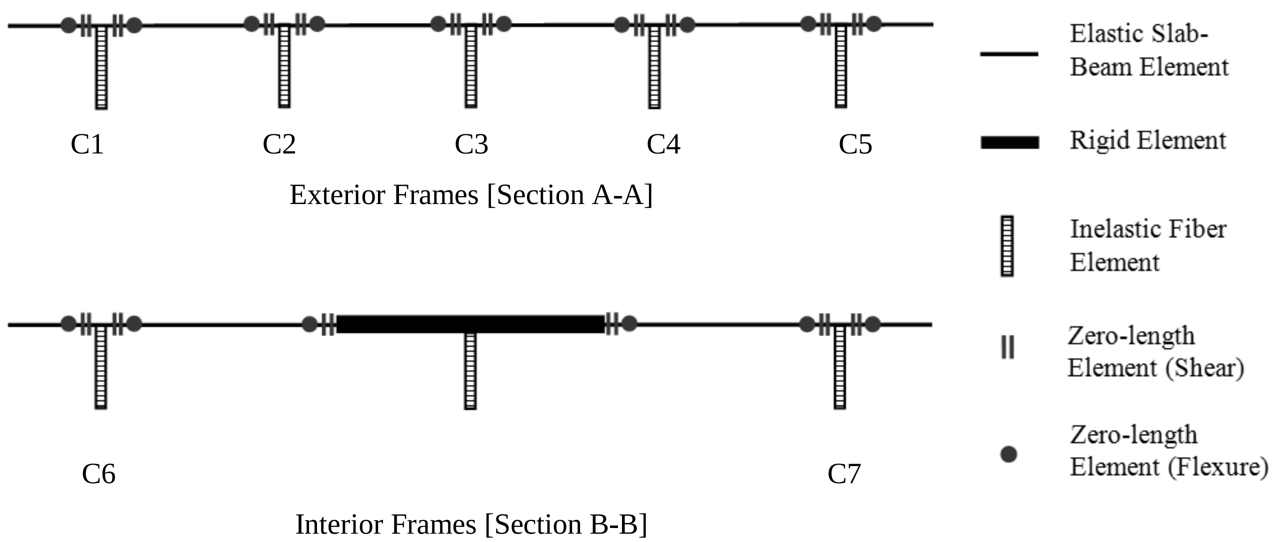

Figure 5-4: Illustration of the Nonlinear Equivalent Frame Components

5.3.2 Materials

The concrete material of all grades was modelled using the 'Concrete01' material embedded in OpenSees. The material model accounts for stiffness degradation in a linear manner as shown in, ignoring the tensile strength of concrete (Figure 5-5).

The fiber sections of core walls and gravity columns accounted for the variation of properties between confined concrete and unconfined concrete based on Mander's model (1988).

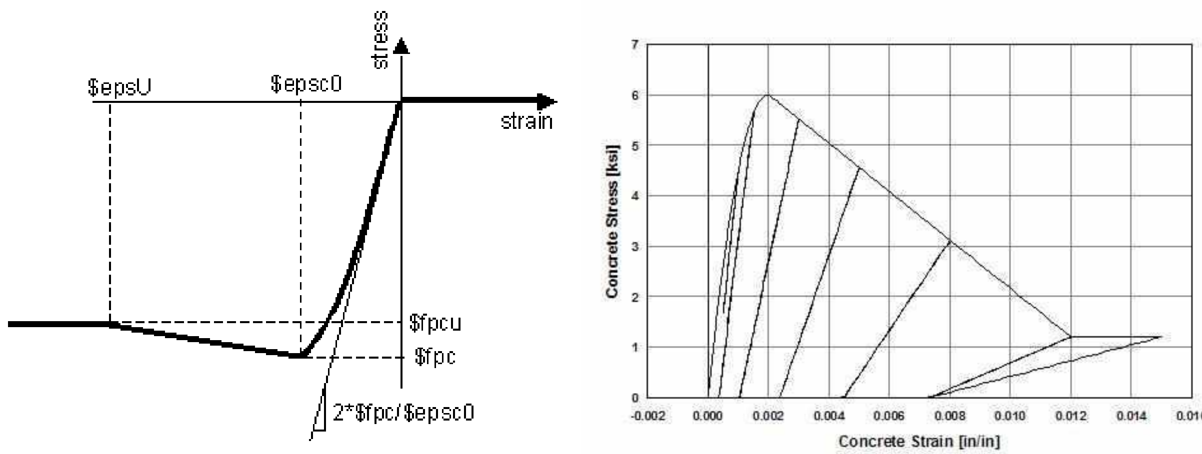

Figure 5-5: Concrete01 Material Model in OpenSees (PEER, 2015)

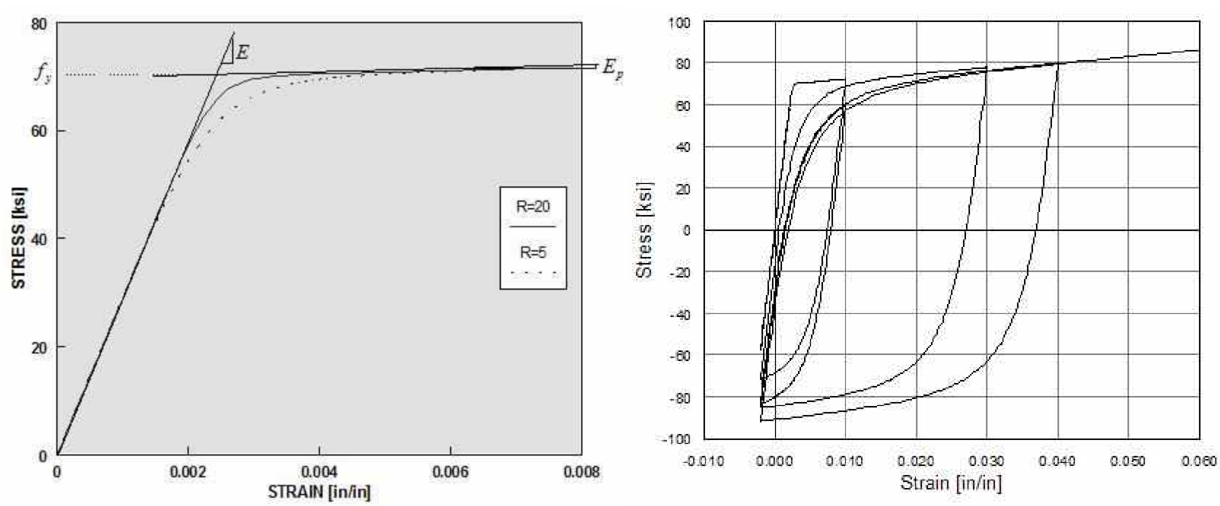

Figure 5-6: Steel02 Material Model in OpenSees (PEER, 2015)

Steel reinforcement of all grades was modelled using the 'Steel02' material. The material is based on Giuffré-Menegotto-Pinto's model with isotropic strain hardening. Figure 5-6 shows the behaviour of the backbone parameters and the hysteretic simulation by the material model.

5.3.3 Selection and Scaling of Ground Motions

Strong historical crustal earthquake ground motions were selected and linearly-scaled from the PEER Strong Motion Database (PEER, 2015b) to match the target design spectrum. The available ground motion records were narrowed down to records between 0 to 200 kilometers from the rupture of earthquake events with moment magnitude between 6 and 8, to reflect the magnitude and distance of Vancouver's main source of hazard. Only ground motions recorded on soil with Vs30 between 560 m/s to 1500 m/s corresponding to site class B and C were considered. As recommended by ASCE7-10, the target matching period range was set to be 0.2 to 1.5 times the fundamental period of the structure under consideration (ASCE, 2010). The reason for matching between a target period range, rather than matching at a specific period, is to capture the uncertainty in the fundamental period, the contribution of higher vibration modes with shorter periods, and the potential lengthening of the fundamental mode due to yielding of structure. The scaling factor was limited between 0.2 and 4.0 to prevent excessive scaling of ground motion which may result in unrealistic ground motions records.

Twelve ground motions were selected with preference on ground motions with lower mean square error (MSE) over the matching period range. The geometric mean of the horizontal fault parallel and fault normal components is used for the linear scaling and matching of ground motions. The selected ground motions along with the corresponding scale factors and other key parameters are summarized in Table 5-2. The target spectrum is plotted in Figure 5-7.

Table 5-2: Selected Ground Motions for 2475 Years Return Period

NGA #		Mean Squared Error	Scale Factor	Event	Year	Mag.	Rrup [km]	Vs30 [m/s]	Mechanism
1	1165	0.025	0.9349	Kocaeli-Turkey	1999	7.51	7.2	811	Strike-Slip
2	284	0.035	4.0000	Irpinia-Italy-01	1980	6.9	9.6	1000	Normal
3	143	0.036	0.3151	Tabas-Iran	1978	7.35	2	767	Reverse
4	2107	0.053	3.3660	Denali-Alaska	2002	7.9	50.9	964	Strike-Slip
5	285	0.126	0.9038	Irpinia-Italy-01	1980	6.9	8.2	1000	Normal
6	957	0.144	3.9057	Northridge-01	1994	6.69	16.9	822	Reverse
7	791	0.052	2.3458	Loma Prieta	1989	6.93	34.3	685	Reverse-Oblique
8	1795	0.053	4.0000	Hector Mine	1999	7.13	50.4	685	Strike-Slip
9	126	0.045	0.4624	Gazli-USSR	1976	6.8	5.5	660	Unkown
10	1154	0.087	2.4237	Kocaeli-Turkey	1999	7.51	65.5	660	Strike-Slip
11	1618	0.093	3.1616	Duzce-Turkey	1999	7.14	8	660	Strike-Slip
12	1626	0.117	4.0000	Sitka-Alaska	1972	7.68	34.6	660	Strike-Slip

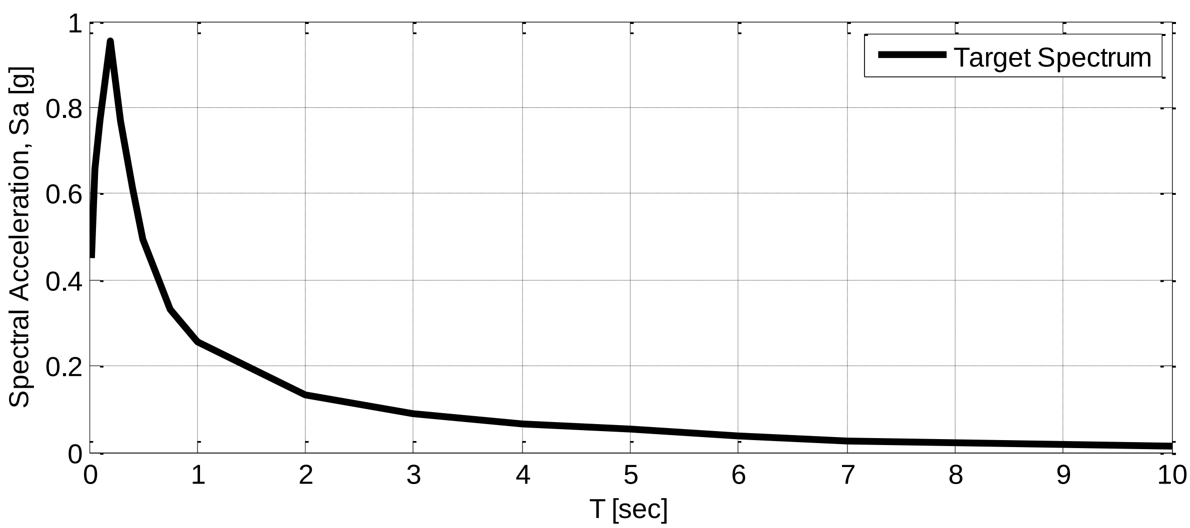

Figure 5-7: Target Spectrum for 2475 Years Return Period

5.4 Case Study [1]

5.4.1 Objectives:

Investigating the effects of including the RCFS system in the analysis model of the prototype building.

5.4.2 Nonlinear Dynamic Analyses and Results

Three sets of analyses with and without the gravity system elements were conducted. Table 5-3 shows a comparison of the structural periods obtained from the three models.

Table 5-3: Comparison of the Fundamental Period and Stiffness by Including the Gravity System Elements

Model	T_i [sec]	Change in Stiffness	
Core Walls [1]	4.38	-	
Core Walls + Columns [2]	4.31	3%	
Core Walls + Columns + Slabs [3]	4.13	12% *	9% **
* Difference between [3] and [1]	** Difference between [3] and [2]		

During the time-history analyses of models 2 and 3 (without and with the RCFS system), the maximum recorded inter-storey drift (ISD) ratios at each storey were recorded. Figure 5-8 shows these maximum ISD ratios due to all ground motions, as well as the median values for each model. Comparisons are presented in Figure 5-9. The maximum recorded demands on the core walls from both models were also plotted (see Figure 5-10), and comparisons are presented in Figure 5-11.

The results obtained from the analyses indicated that earthquake demands on the exterior gravity columns are higher than those on the interior columns. Hence, columns C1 and C6 (as annotated in Figure 5-3) were selected for comparing the demands (see Figure 5-12).

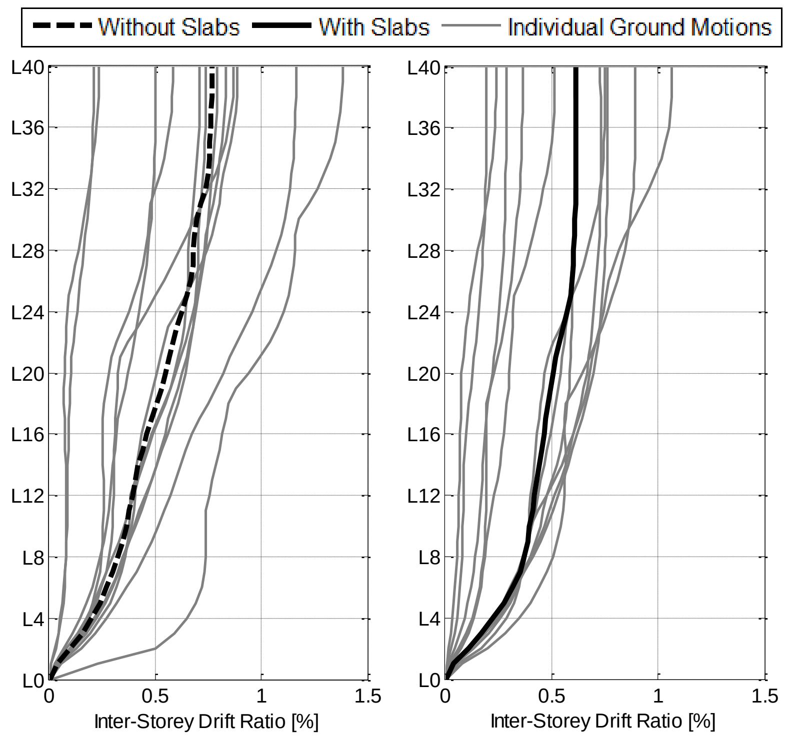

Figure 5-8: Inter-Storey Drift Ratios

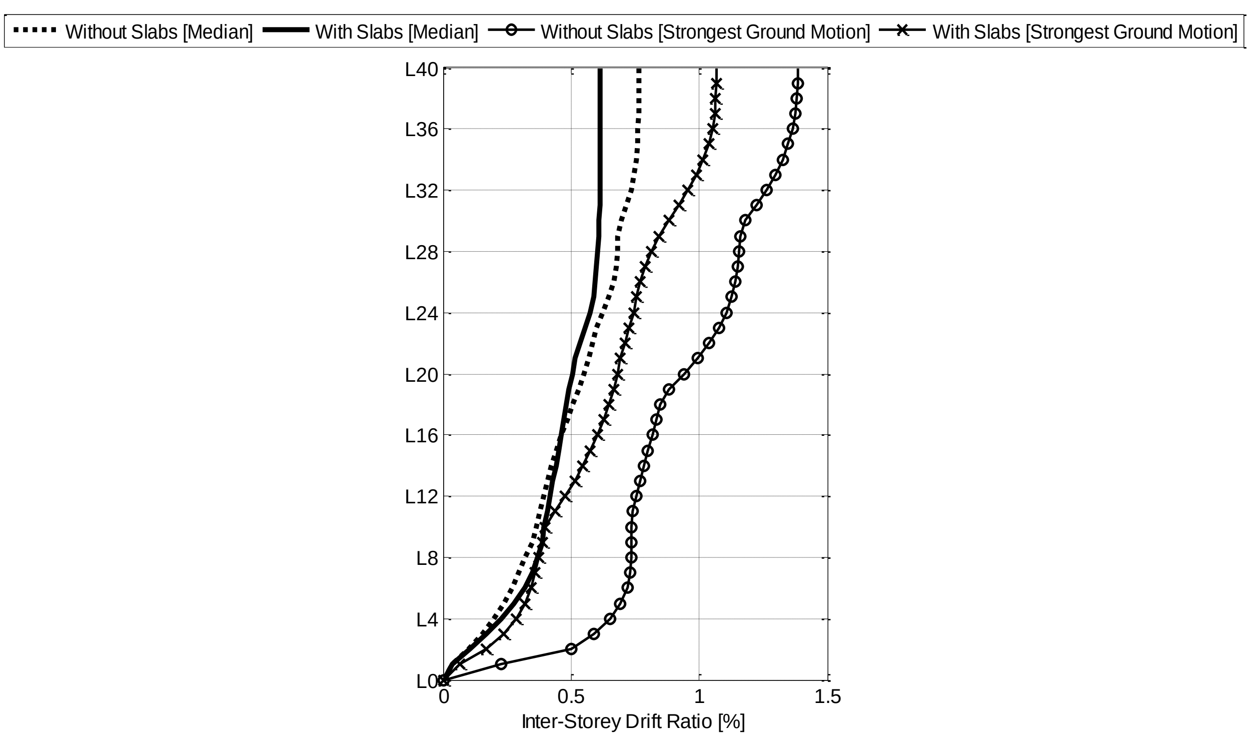

Figure 5-9: Comparison between Inter-Storey Drift Ratios [Median and Strongest Ground Motion]

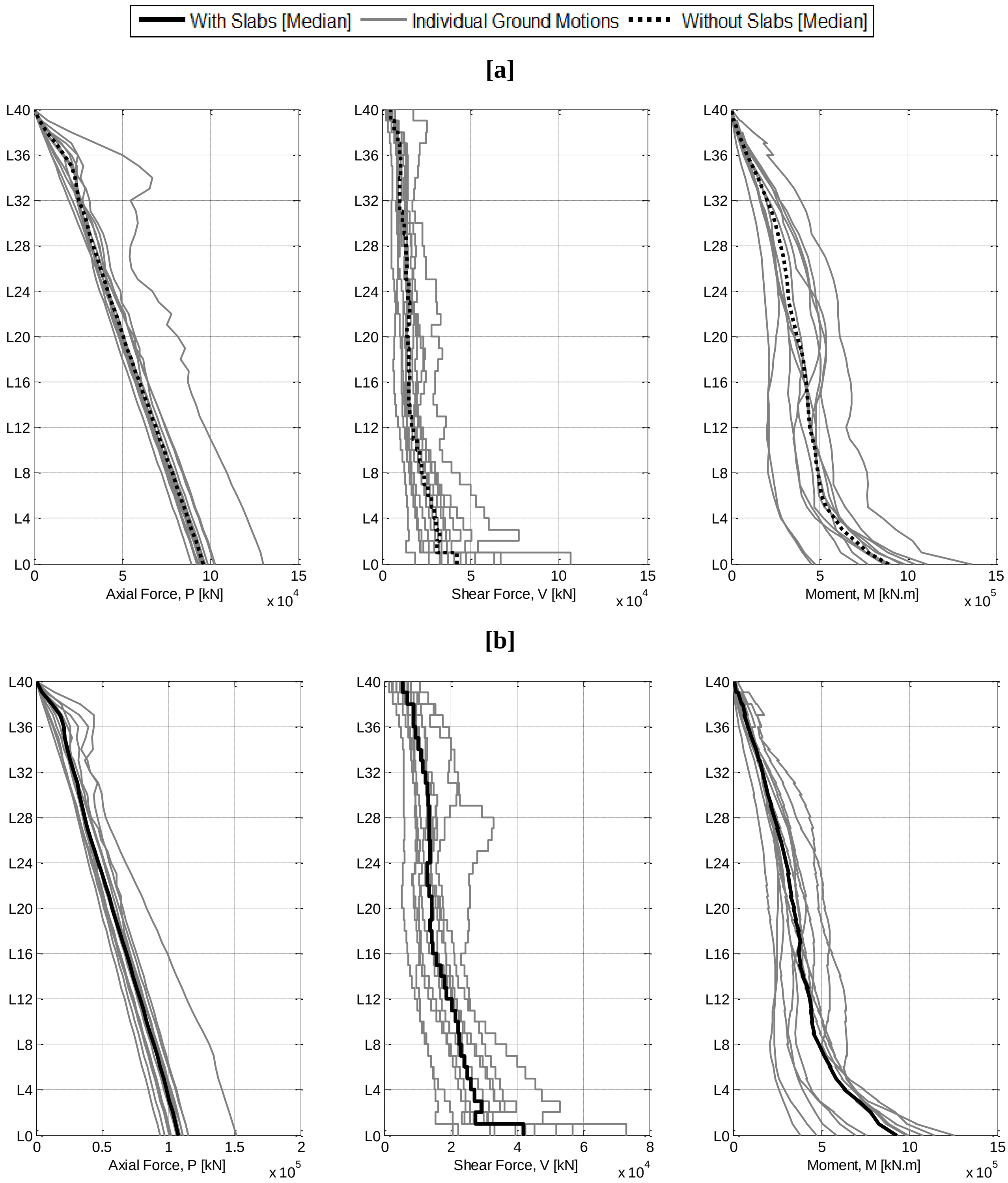

Figure 5-10: Total Demands on Core Walls from the Two Analyses Models - [a] Model Without Slabs; [b] Model With Slabs

[a]

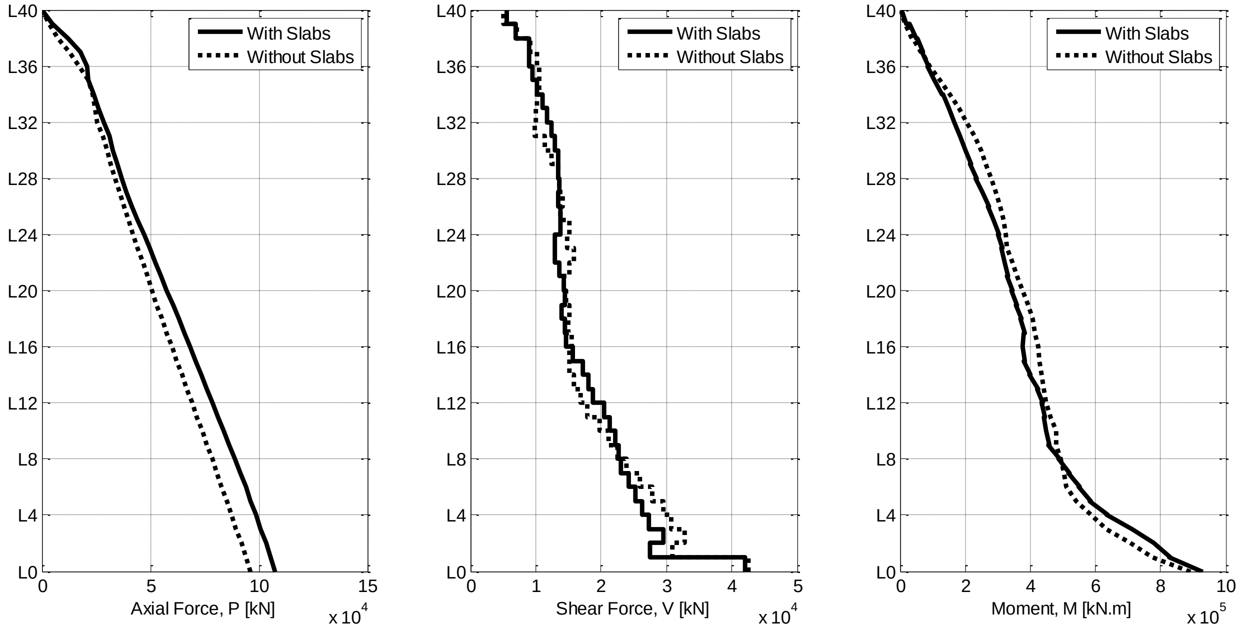

[b]

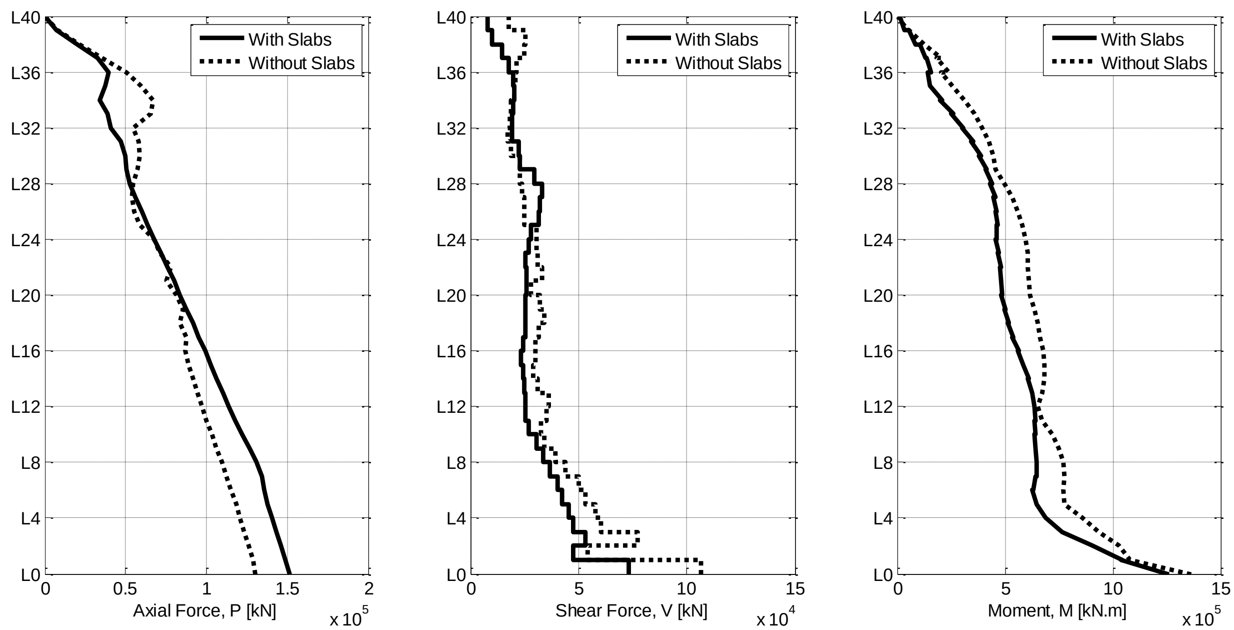

Figure 5-11: Comparison between Demands on Core Walls - [a] Median of 12 Ground Motion; [b] Strongest Ground Motion

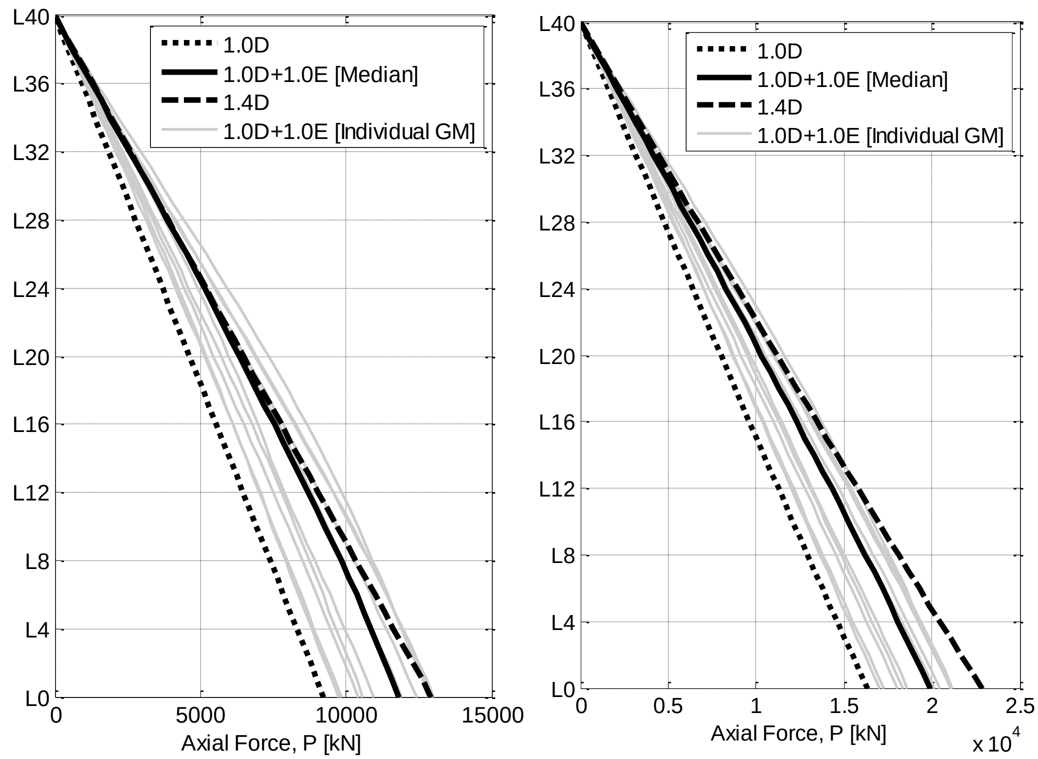

Figure 5-12: Axial Demands on Critical Gravity Columns

5.4.3 Discussion

The results show that adding the gravity columns to the model increases the overall lateral stiffness of the structure by 3%. On the other hand, when both the columns and the RCFS system are modeled, the lateral stiffness of the structure increases by about 12%.

The comparison the ISD results (see Figure 5-9) shows that modeling the RCFS system has a significant influence in the estimated inter-story drifts the structure undergoes. The maximum ISD ratio recorded from time-history analyses reduces by 19.7% [median] and 23.2% [strongest ground motion] when the RCFS elements are added.

The median results (see Figure 5-11a) suggest that modeling the RCFS system leads to an increase of 12.1% in the axial demands on the core walls. Though, the effects on the shear and flexural responses are negligible. However, when the structure is subjected to the strongest ground motion, the results (see Figure 5-11b) show significant changes up to 47.4%, 31.6%, and 20.4% in axial, shear, and flexural responses, respectively. Similarly, the inclusion of the RCFS system increases the axial force on the critical gravity columns by up to 28.1% [median] and 40.8% [strongest ground motion].

Based on these comparisons, it is recommended to include the RCFS in the analysis model to obtain a more realistic estimates of the structural responses, and capture the interaction between the SFRS and the GS.

5.5 Case Study [2]

5.5.1 Objectives:

1) Investigating the effects of alternative RCFS designs on the global seismic response of the prototype building.
2) Verifying the capability of the proposed model to detect local failures at the FSC connections during time-history analyses.

5.5.2 Nonlinear Dynamic Analyses and Results

<u>Objective #1:</u>

To address the first objective of the case study, a parametric study was conducted on the prototype building to study how the thickness of the flat slabs impacts the overall structural performance. The RCFS system was re-designed for thicknesses of 250 mm and 300 mm, satisfying the design requirements by CSA A23.3 (2014). The nonlinear model was modified accordingly to account for the changes in mass, gravity loads, equivalent slab-beams, and plastic hinge properties in each case.

The analytical results indicated that the changes in the building's structural period were insignificant when the thickness of the slabs was changed to 250 mm and 300 mm.

The maximum recorded ISD ratios at each storey were plotted for each case (see Figure 5-13). Comparisons between the median and the strongest ground motion results are presented in Figure 5-14.

Similarly, the total demands on the core walls obtained from the models with 250 mm slabs and 300 mm slabs were plotted in Figure 5-15a and Figure 5-15b, respectively. Comparisons to the median and the strongest ground motion results from the original model (with 200 mm slabs) are shown in Figure 5-16.

It should be noted that the comparison plots focus on the 10 floor levels at which the maximum differences occur.

<u>Objective #2:</u>

To address the second objective of the case study, the RCFS system was again re-designed with 300 mm slabs and no shear reinforcement, such that the FSC connections have low resistance to drift-induced punching shear. The deformation capacity of the FSC connections without shear reinforcement were determined based on the experimental data compiled by Kang and Wallace (2006).

The behaviour of the FSC connections from the two models (with brittle connections and with ductile connections) were compared when the structure was subjected to the strongest ground motion. Throughout the time-history analysis, punching shear failures were detected at all FSC connections from floor level 22 up to floor level 40. Figure 5-17 shows the moment-rotational response of the FSC connection at column C6 of the 40th floor in both cases. The total axial force demands on the core walls were also compared to ensure that the brittle connections do not contribute to the global structural response after punching shear failures.

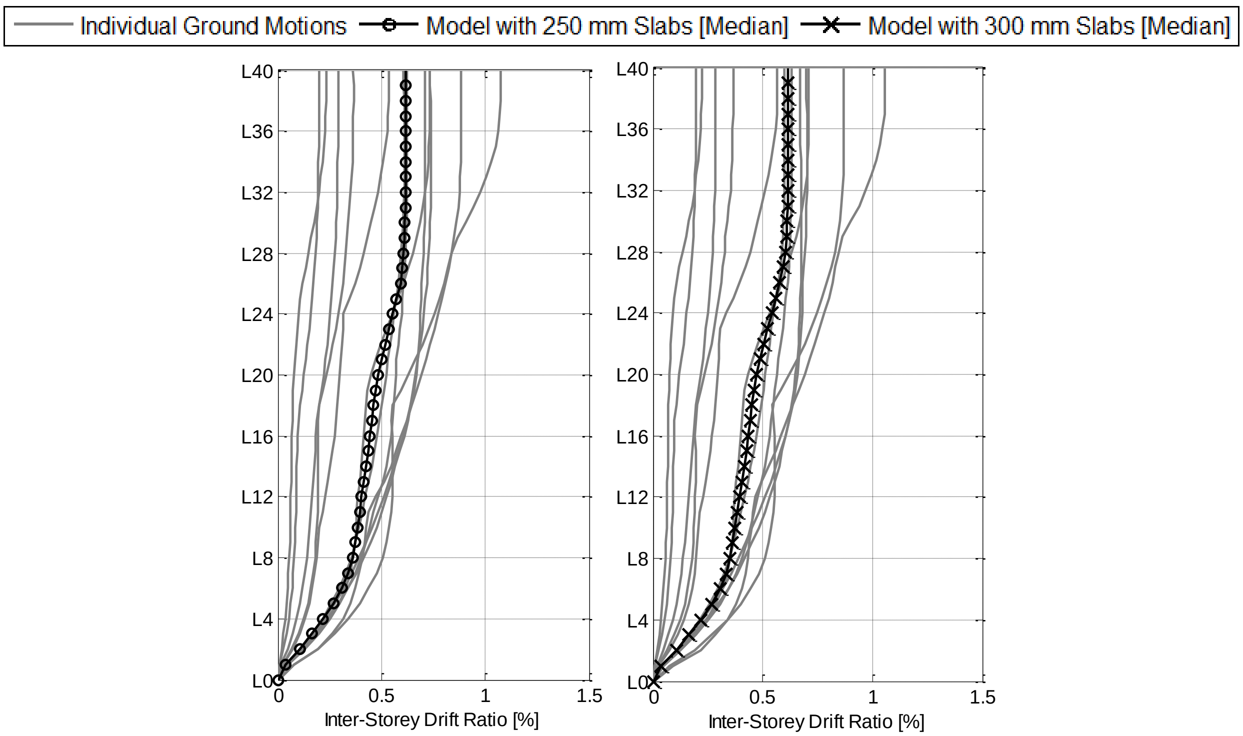

Figure 5-13: Inter-Storey Drift Ratios Obtained from Models with 250 mm and 300 mm Slabs

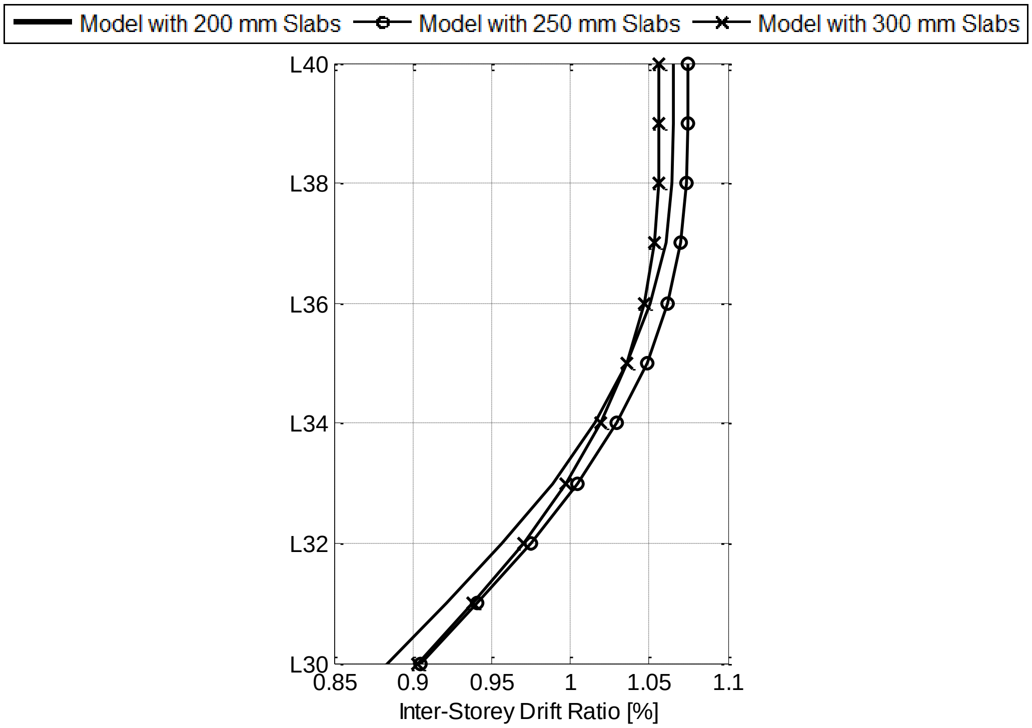

Figure 5-14: Comparison between Inter-Storey Drift Ratios - Strongest Ground Motion

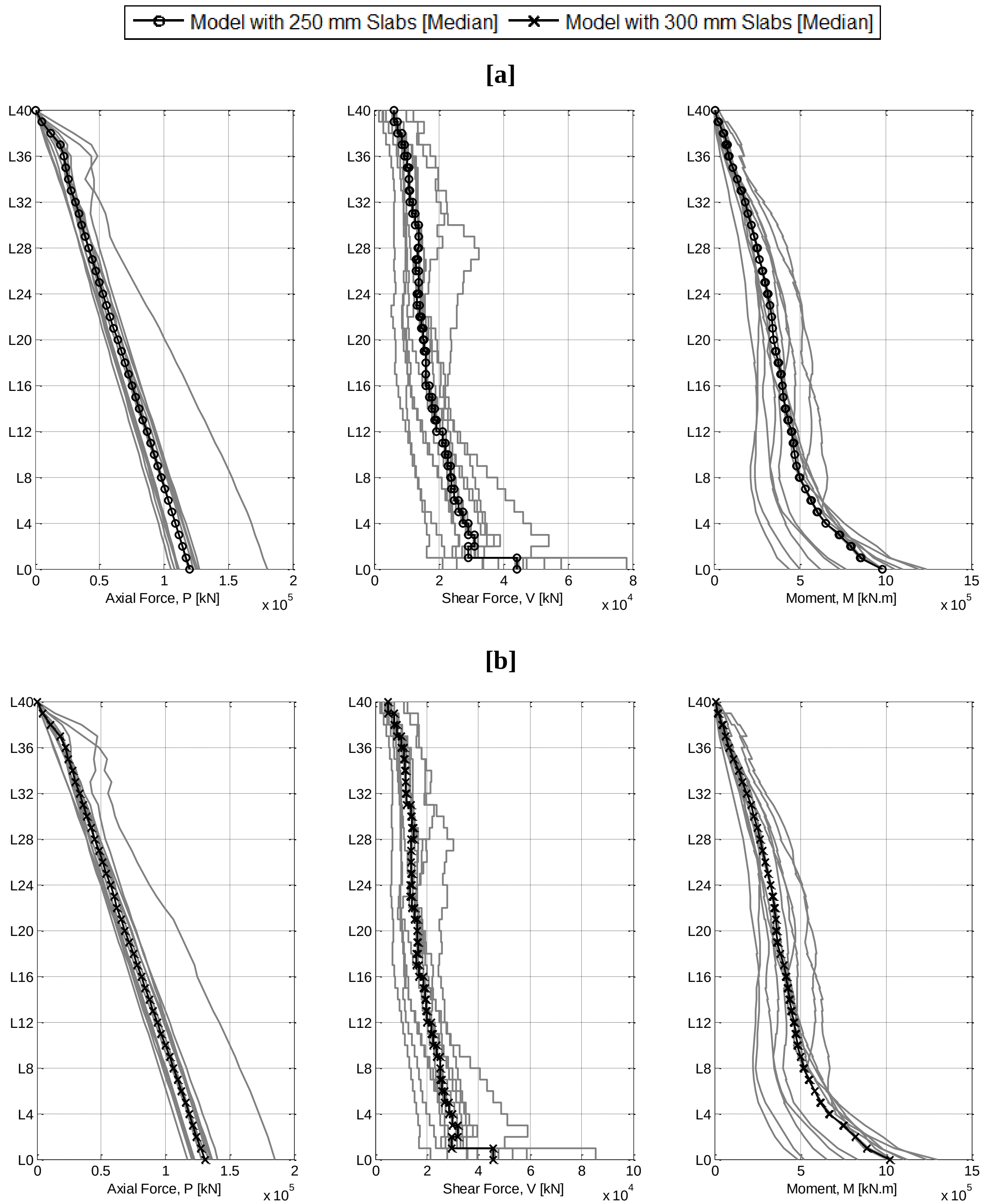

Figure 5-15: Total Demands on Core Walls - [a] Model with 250 mm Slabs; [b] Model with 300 mm Slabs

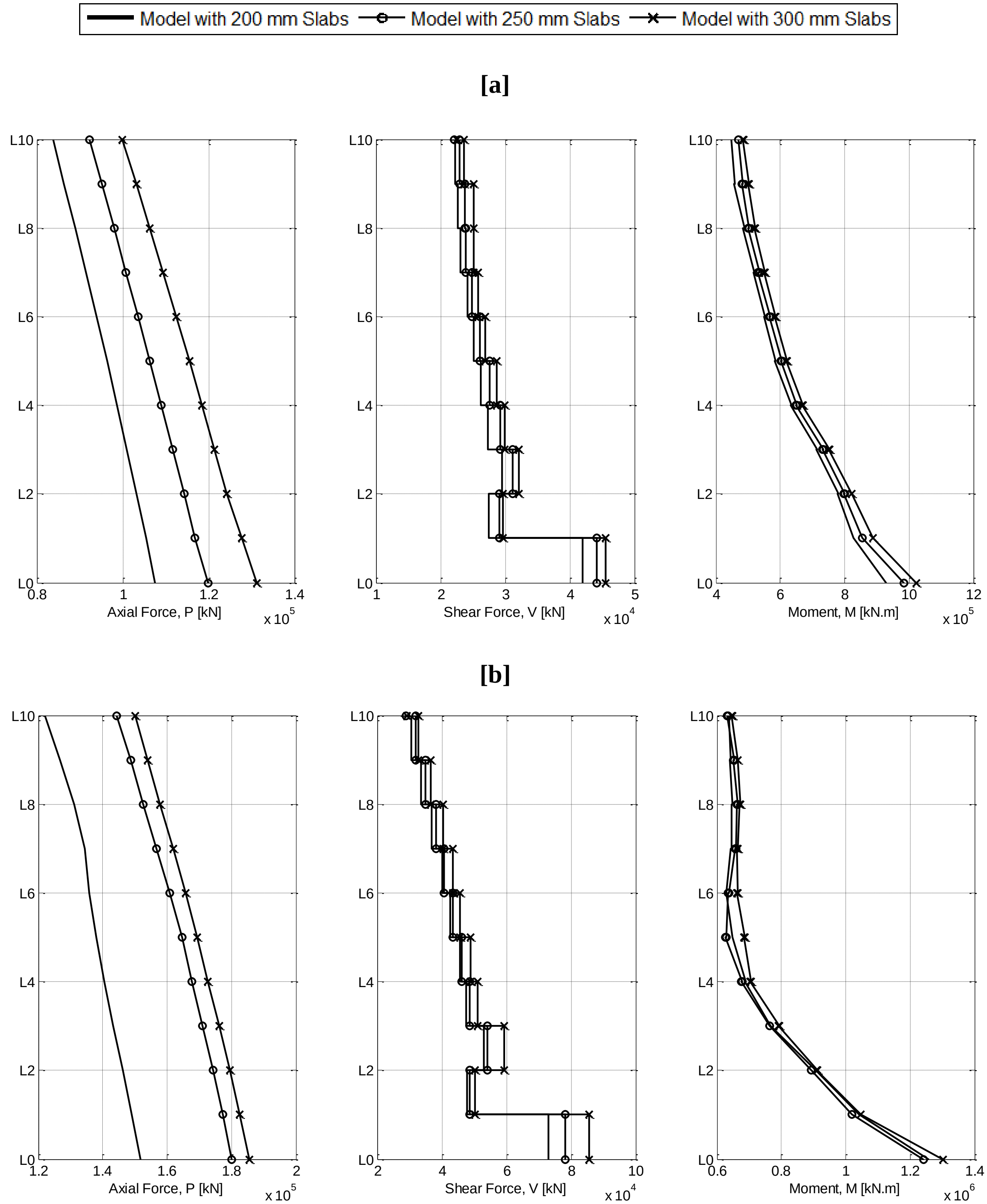

Figure 5-16: Comparison between Demands on Core Walls for Models with Different Slab Thicknesses - [a] Median; [b] Strongest Ground Motion

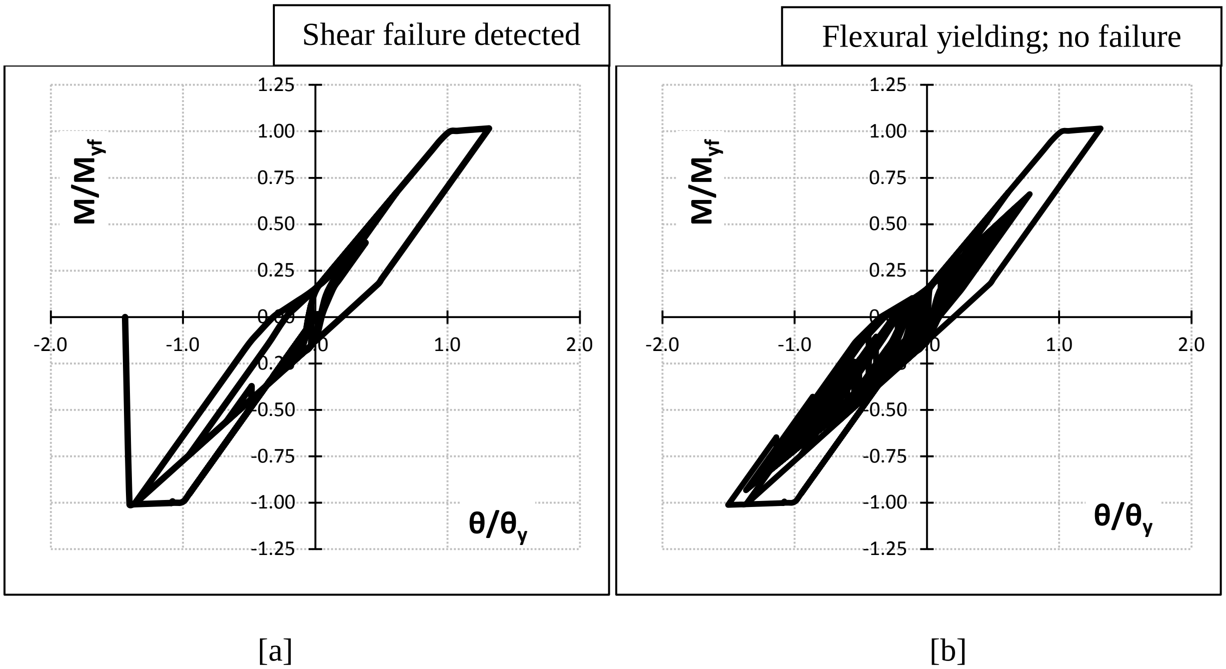

Figure 5-17: Normalized Moment-Rotation Responses [a] Brittle Connection; [b] Ductile Connection

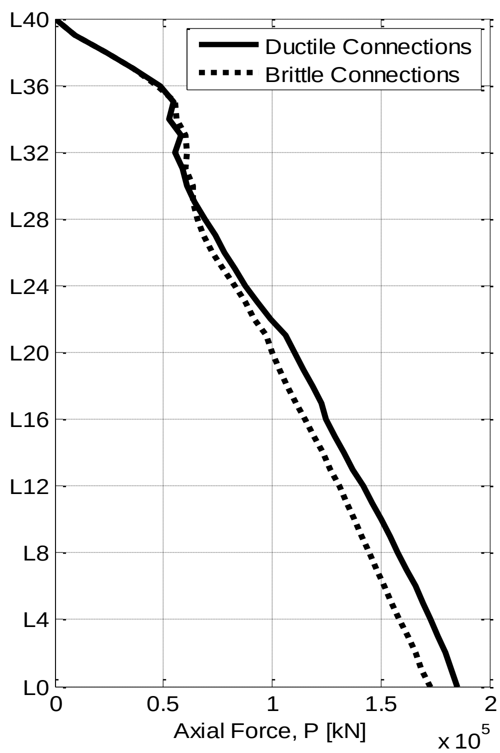

Figure 5-18: Comparison between the SFRS Axial Demands Using Ductile Connections vs. Brittle Connections

5.5.3 Discussion

Increasing the thickness of flat slabs within the practical design range was found not to have a significant impact on the structural period of the building. This is because the increases in the overall lateral stiffness, due to larger slab thicknesses, were compensated by the imposed larger masses. The changes in the maximum recorded ISD ratios were also insignificant, even when the structure was subjected to the strongest ground motion (see Figure 5-14).

By comparing the SFRS demands using three different RCFS designs (see Figure 5-16), substantial increases in the axial demands due to using thicker slabs can be observed. The shear demands are also increased when thicker flat slabs are used. The results plotted in Figure 5-16b suggest that the differences in these demands increase when the structure undergoes higher ISD ratios. On the other hand, the comparison between the overturning moment demands did not show significant increases when the slabs were differently designed.

When the RCFS system was designed with brittle connections, the proposed model was capable of capturing the punching shear failure that occurred at multiple locations in the structure. The structural response verified that once local FSC connection failures are detected, the corresponding flat slab elements no longer contribute to the overall strength and stiffness of the structure.

Chapter 6: Conclusions

6.1 Summary

The RCFS system is commonly utilized in high-rise construction in North America. The design of flat slabs is usually governed by gravity demands, while the effects of seismic demands are not directly considered. Additionally, when assessing the seismic performance of a structure, the influence of the RCFS system and the gravity columns is traditionally ignored.

With increasing trends in performance-based design, developing robust nonlinear finite element models is becoming a crucial step in the design process. Including the RCFS system in the analysis model is therefore important to obtain better estimates of the structural responses, and a realistic interaction between the SFRS and the GS.

A spectrum of experimental and analytical studies on the behaviour of RC flat slabs when subjected to combined gravity and lateral loads were reviewed. Outcomes from these studies indicate that the response of flat slabs is mainly governed by the behaviour of FSC connections. Therefore, a new lumped-plasticity model that is capable of simulating the nonlinear behaviour of FSC connections with shear reinforcement was developed. This is because the existing nonlinear models are unable to accurately capture the hysteretic response and failures of ductile FSC connection. The proposed model was verified and calibrated using data from actual experimental tests.

Two case studies were conducted to investigate: [1] the effects of including the RCFS system in the analysis model of a typical 40-storey concrete shear wall building, and [2] the influence of different RCFS designs on the global structural responses.

The results from nonlinear dynamic analyses proved that modeling the RCFS system has significant impacts on the estimated structural responses, as well as the force demands on both the SFRS and the GS. Using flat slabs with larger thicknesses resulted in increased force demands on the structural system, with substantial increases in the axial forces in particular. However, the structural period and the maximum ISD ratios were found not to be sensitive to the thickness changes in the RCFS system.

Furthermore, it was verified that the proposed model is capable of detecting local FSC connection failures throughout time-history dynamic analyses, accounting for the loss in the overall strength and stiffness of the structure in subsequent analysis results. The type of failure mode of the FSC connections was found not to have a significant impact neither on the SFRS shear and overturning moment demands, nor on the maximum ISD ratios. However, the flexural yielding mode of ductile FSC connections resulted in increased axial demands on the SFRS in comparison with the punching shear mode of brittle connections.

6.2 Recommendations for Future Research

The historical experimental studies have enabled researchers and engineers to understand the seismic behaviour of FSC connections to a large extent. Yet, more studies are encouraged to mitigate the limitations of those studies, and further develop the existing analytical models. Based on the review of experimental studies covered in *Chapter 2*, the following shortcomings were noted:

- The test specimens in some existing experimental studies might not fully represent the behaviour of FSC connections in real buildings. For example, exaggerated punching shear capacities could have been obtained from the experimental program by Megally and Ghali (2000) due to the use of relatively high longitudinal tensile reinforcement ratios. According to Widianto et al. (2009), improved shear strength and reduced longitudinal reinforcement strains are obtained when the amount of flexural reinforcement is increased within the flexure-transfer width.

- The vast majority of experiments were conducted on FSC connections with rectangular columns. Extensive studies on slab connections with circular columns and walls are required to validate the existing analytical models and code provisions.

- Most experimental studies on FSC connections with shear reinforcement were conducted using static cyclic loads in one directions. This method may result in underestimated resistances of the FSC connections to drift-induced punching shear. Therefore, bi-directional dynamic tests are required to determine more realistic maximum deformation limits for FSC connections with different types of shear reinforcement.

- A limited number of experimental studies have included specimens with corner FSC connections. Therefore, more experimental data for corner FSC connections with shear reinforcement are required to verify the existing code provisions.

Bibliography

ACI 318 COMMITTEE (2011). Building Code Requirements for Structural Concrete (ACI 318-11) and Commentary, *American Concrete Institute* 2011.

ACI 318 COMMITTEE (2014). Building Code Requirements for Structural Concrete (ACI 318-14) and Commentary, *American Concrete Institute*.

ACI-ASCE 352 JOINT COMMITTEE (2011). Guide for Design of Slab-Column Connections in Monolithic Concrete Structures (ACI 352.1R-11), *American Concrete Institute*.

ACI-ASCE 421 JOINT COMMITTEE (2010). Guide to Seismic Design of Punching Shear Reinforcement in Flat Plates (ACI 421.2R-10), *American Concrete Institute*.

ASCE (2010). Minimum Design Loads for Buildings and Other Structures (ACSE/SEI 7-10). *American Society of Civil Engineers*.

BANCHIK, C.A. (1987). Effective beam width coefficients for equivalent frame analysis of flat-plate structures. *ME Thesis, Department of Civil and Environmental Engineering, The University of California, Berkeley*.

BROMS, C.E. (1990). Punching of flat plates - A question of concrete properties in biaxial compression and size effect. *ACI Structural Journal,* **87**(3).

BROMS, C.E. (2000). Elimination of flat plate punching failure mode. *ACI Structural Journal,* **97**(1).

CHOI, K., SHIN, D. and PARK, H. (2014a). Modification of the ACI 318 Design Method for Slab-Column Connections Subjected to Unbalanced Moment. *Advances in Structural Engineering*, **17**(10), pp. 1469-1480.

CHOI, K., SHIN, D. and PARK, H. (2014b). Shear-Strength Model for Slab-Column Connections Subjected to Unbalanced Moment (with Appendix). *ACI Structural Journal,* **111**(3).

CORLEY, W.G. and JIRSA, J.O. (1970). Equivalent frame analysis for slab design. *ACI Journal Proceedings (Vol. 67, No. 11).*

CORLEY, W.G., SOZEN, M. and SIESS, C. (1961). The equivalent frame analysis for reinforced concrete slabs. *ACI Journal Proceedings*.

CSA A23.3 COMMITTEE. (2004). Design of Concrete Structures: A National Standard of Canada. *Canadian Standards Association.* Rexdale, Canada.

CSA A23.3 COMMITTEE. (2014). Design of Concrete Structures: A National Standard of Canada. *Canadian Standards Association.* Rexdale, Canada.

DI STASIO SR, J. and VAN BUREN, M. (1960). Transfer of bending moment between flat plate floor and column. *ACI Journal Proceedings*.

DILGER, W.H. and BROWN, S.J. (1995). Earthquake Resistant Slab-Column Connections. *Institut für Baustatik und Konstruction, ETH Zürich*. September, pp. 22-27.

DILGER, W.H. and CAO, H. (1992). Behavior of slab-column connections under reversed cyclic loading. *Proc., 2nd Int. Conf. on High-Rise Buildings in Nanjing, China*. Council of Tall Buildings and Urban Habitat, Chicago, 212–224.

ELGABRY, A.A. and GHALI, A. (1987). Tests on Concrete Slab-Column Connections with Stud-Shear Reinforcement Subjected to Shear-Moment Transfer. *ACI Structural Journal,* **84**(5).

ELGABRY, A.A. and GHALI, A. (1996a). Moment transfer by shear in slab-column connections. *ACI Structural Journal,* **93**(2).

ELGABRY, A.A. and GHALI, A. (1996b). Transfer of moments between columns and slabs: Proposed code revisions. *ACI Structural Journal,* **93**(1).

EL-SALAKAWY, E.F., POLAK, M.A. and SOLIMAN, M.H. (2000). Reinforced concrete slab-column edge connections with shear studs. *Canadian Journal of Civil Engineering,* **27**(2), pp. 338-348.

FARHEY, D.N., YANKELEVSKY, D.Z. and ADIN, M.A. (1997). Resistance mechanism model for reinforced concrete flat slab-column frame connections. *ACI Structural Journal,* **94**(6).

GAYED, R.B. and GHALI, A. (2008). Seismic design of concrete slabs for punching shear: a critical review of Canadian standard CSA A23.3-04. *Canadian Journal of Civil Engineering,* **35**(6), pp. 588-599.

GROSSMAN, J.S. (1997). Verification of proposed design methodologies for effective width of slabs in slab-column frames. *ACI Structural Journal,* **94**(2).

HAN, S.W., PARK, Y. and KEE, S. (2009). Stiffness reduction factor for flat slab structures under lateral loads. *Journal of Structural Engineering*.

HANSON, N.W. and HANSON, J.M. (1968). Shear and moment transfer between concrete slabs and columns. *J. Portland Cement Ass. Res. Develop. Lab,* **10**(1), pp. 2-16.

HAWKINS, N.M., MITCHELL, D. and HANNA, S.N. (1975). The effects of shear reinforcement on the reversed cyclic loading behavior of flat plate structures. *Canadian Journal of Civil Engineering,* **2**(4), pp. 572-582.

HUESTE, M.B.D., BROWNING, J., LEPAGE, A. and WALLACE, J.W. (2007). Seismic design criteria for slab-column connections. *ACI Structural Journal,* **104**(4).

HUESTE, M.B.D., KANG, T.H. and ROBERTSON, I.N. (2009). Lateral Drift Limits for Structural Concrete Slab-Column Connections Including Shear Reinforcement Effects, *Structures Congress 2009,* ASCE, pp. 1-10.

HUESTE, M.B.D. and WIGHT, J.K. (1999). Nonlinear punching shear failure model for interior slab-column connections. *Journal of Structural Engineering,* **125**(9), pp. 997-1008.

HWANG, S. and MOEHLE, J.P. (1990). Experimental study of flat-plate structures under vertical and lateral loads. *NISEE E-Library, The University of California, Berkeley*.

HWANG, S. and MOEHLE, J.P., (2000a). Vertical and lateral load tests of nine-panel flat-plate frame. *ACI Structural Journal*, **97**(1).

HWANG, S. and MOEHLE, J.P. (2000b). Models for laterally loaded slab-column frames. *ACI Structural Journal*, **97**(2).

ISLAM, S. and PARK, R. (1976). Tests on Slab Column Connections with Shear and Unbalanced Flexure. *ASCE, Journal of the Structural Division*, Vol. 102, No. ST3, pp. 549-568.

IVY, C.B., IVEY, D.L., and BUTH, E. (1969). Shear Capacity of lightweight concrete flat slabs. *ACI Journal Proceedings (Vol. 66, No. 6).*

JIRSA, J., SOZEN, M.A., and SIESS, C.P. (1963). The Effects of Pattern Loadings on Reinforced Concrete Floor Slabs. *Structural Research Series No. 269, Department of Civil Engineering, University of Illinois.*

KANG, T.H. (2004). Shake table tests and analytical studies of reinforced and post-tensioned concrete flat plate frames. *PhD Thesis, Department of Civil Engineering, The University of California, Los Angeles*.

KANG, T.H. and WALLACE, J.W. (2005). Dynamic responses of flat plate systems with shear reinforcement. *ACI Structural Journal,* **102**(5).

KANG, T.H. and WALLACE, J.W. (2006). Punching of reinforced and post-tensioned concrete slab-column connections. *ACI Structural Journal*, **103**(4).

KANG, T.H., WALLACE, J.W. and ELWOOD, K.J. (2009). Nonlinear modeling of flat-plate systems. *Journal of Structural Engineering,* **135**(2), pp. 147-158.

LUO, Y. and DURRANI, A. (1995a). Equivalent Beam Model for Flat-Slab Buildings: Part I: Interior Connections. *ACI Structural Journal*, **92**(1).

LUO, Y. and DURRANI, A. (1995b). Equivalent Beam Model for Flat-Slab Buildings: Part II: Exterior Connections. *ACI Structural Journal*, **92**(1).

LUO, Y., DURRANI, A. and CONTE, J. (1994). Equivalent frame analysis of flat plate buildings for seismic loading. *Journal of Structural Engineering,* **120**(7), pp. 2137-2155.

MANDER, J.B., PRIESTLEY, M.J. and PARK, R. (1988). Theoretical stress-strain model for confined concrete. *Journal of Structural Engineering,* **114**(8), pp. 1804-1826.

MARTI, P. and KONG, K. (1987a). Response of reinforced concrete slab elements to torsion. *Journal of Structural Engineering,* **113**(5), pp. 976-993.

MARTI, P., LEESTI, P. and KHALIFA, W.U. (1987b). Torsion tests on reinforced concrete slab elements. *Journal of Structural Engineering,* **113**(5), pp. 994-1010.

MARTINEZ-CRUZADO, J.A. (1993). Experimental study of post-tensioned flat plate exterior slab-column connections subjected to gravity and biaxial loading. *PhD Thesis, Department of Civil and Environmental Engineering, The University of California, Berkeley*.

MEGALLY, S. and GHALI, A. (1996). Nonlinear analysis of moment transfer between columns and slabs, *Proceedings, Vol. IIa. Canadian Society of Civil Engineering Conference, Edmonton, Alberta, Canada* 1996, pp. 321-332.

MEGALLY, S. and GHALI, A. (2000). Seismic behavior of edge column-slab connections with stud shear reinforcement. *ACI Structural Journal*, **97**(1).

MEGALLY, S. and GHALI, A. (1994). Design considerations for slab-column connections in seismic zones. *ACI Structural Journal,* **91**(3).

MOEHLE, J.P. (1988). Strength of slab-column edge connections. *ACI Structural Journal,* **85**(1).

MOEHLE, J.P. and DIEBOLD, J.W. (1985). Lateral load response of flat-plate frame. *Journal of Structural Engineering,* **111**(10), pp. 2149-2164.

MOWRER, R.D., and VANDERBILT, M.D. (1967). Shear strength of lightweight aggregate reinforced concrete flat plates. *ACI Journal Proceedings (Vol. 64, No. 11).*

NBCC (2010). National Building Code of Canada. *Canadian Commission on Building and Fire Codes, Institute for Research in Construction*. Ottawa, Ontario.

OSMAN, M., MARZOUK, H., and HELMY, S. (2000). Behavior of high-strength lightweight concrete slabs under punching loads. *ACI Structural Journal,* **97**(3).

PAN, A.P., PAN, A.A. and MOEHLE, J.P. (1988). Reinforced concrete flat plates under lateral loading: An experimental study including biaxial effects. *Earthquake Engineering Research Center, University of California, Berkeley*.

PAN, A. and MOEHLE, J.P. (1989). Lateral displacement ductility of reinforced concrete flat plates. *ACI Structural Journal,* **86**(3).

PAN, A.D. and MOEHLE, J.P. (1992). An experimental study of slab-column connections. *ACI Structural Journal,* **89**(6).

PARK, H. and CHOI, K. (2006). Improved strength model for interior flat plate–column connections subject to unbalanced moment. *Journal of Structural Engineering*.

PARK, H. and CHOI, K. (2007). Strength of exterior slab–column connections subjected to unbalanced moments. *Engineering Structures*, **29**(6), pp. 1096-1114.

PARK, H., KIM, Y., SONG, J., KIM, S. and LEE, C. (2007). Lattice Shear Reinforcement for Slab-Column Connection Subjected to Unbalanced Moment. *Journal of the Korea Concrete Institute*, **19**(3), pp. 301-312.

PARK, H., KIM, Y., SONG, J. and KANG, S. (2011). Lattice Shear Reinforcement for Enhancement of Slab-Column Connections. *Journal of Structural Engineering*, **138**(3), pp. 425-437.

PECKNOLD, D.A. (1975). Slab Effective Width for Equivalent Frame Analysis, *ACI Journal Proceedings*.

PEER (2015a). OpenSees command language manual, Version 2.4.6. *Pacific Earthquake Engineering Research Center, USA.*

PEER (2015b). Strong Ground Motion Database. *Pacific Earthquake Engineering Research Center, USA.*

RHA, C., KANG, T.H., SHIN, M. and YOON, J.B. (2014). Gravity and lateral load-carrying capacities of reinforced concrete flat plate systems. *ACI Structural Journal*, **111**(4).

RITCHIE, M., GHALI, A., DILGER, W. and GAYED, R.B. (2006). Unbalanced moment resistance by shear in slab-column connections: experimental assessment. *ACI Structural Journal*, **103**(1), pp. 74.

ROBERTSON, I.N. and DURRANI, A.J. (1993). Gravity load effect on seismic behavior of interior slab-column connections. *ACI Structural Journal*, **89**(1).

ROBERTSON, I.N., KAWAI, T., LEE, J. and ENOMOTO, B. (2002). Cyclic testing of slab-column connections with shear reinforcement. *ACI Structural Journal*, **99**(5).

ROBERTSON, I.N. and JOHNSON, G. (2006). Cyclic lateral loading of nonductile slab-column connections. *ACI Structural Journal*, **103**(3).

SEZEN, H. (2002). Seismic behavior and modeling of reinforced concrete building columns. *PhD Thesis, Department of Civil and Environmental Engineering, The University of California, Berkeley*.

VANDERBILT, M.D. and CORLEY, W.G. (1983). Frame analysis of concrete buildings. *Concrete International*, **5**(12), pp. 33-43.

WIDIANTO, O.B. and JIRSA, J.O. (2009). Two-way shear strength of slab-column connections: Re-examination of ACI 318 provisions. *ACI Structural Journal*, **106**(2).

WIGHT, J.K. and MACGREGOR, J.G. (2012). *Reinforced Concrete Mechanics and Design, 6th Edition*. New Jersey: Pearson Education, Inc.

YOUSSEF, M.A., MESHALY, M.E. and CHOWDHURY, A.O. (2014). Lateral stiffness of reinforced concrete interior flat plate connections. *Engineering Structures*, **62**, pp. 23-32.

Appendix

Description of the Prototype Building

Usage:		Residential (4F-40F)			
		Commercial (1F-3F)			
Material:		Reinforced concrete shear wall with flat slab and blade wall (gravity column)			
Number of Stories:		40 above ground + 1 Mech. on roof + 4 under ground			
Story Height:		4P-P1 (at 2.75m) 1F (at 4.5m) 2-3F (at 4m) 4-40F (at 3m) Mech. (at 3m)			
Total Height:		126.5 m above ground			
		11 m under ground			
Tower Footprint:		22.5m x 33m			
Mech. on Roof Footprint:		9.6m x 9.6m			
Podium:					
	Footprint:	40m x 58.35m			
	Seismic Joint:	None			
Design Loads:		LL	SDL	SL	Note
	Residential floors	1.92 kPa	1.44 kPa		Residential loading used for tower floors (lvl 4+)
	Residential balconies	4.80 kPa	0.24 kPa		Currently assuming no balconies - these can be added as cantilevers to specific column trib. areas
	Parking	2.40 kPa	0.24 kPa		Parking loading used for levels P1,P2,P3,P4

	Stairs/Corridor	4.80 kPa	0.00 kPa		Corridor loading used for lobby/stair areas within core and (2) 4.5'x31.5' corridors outside of core
	Commercial floors	4.80 kPa	0.48 kPa		Commercial loading used for podium floors
	Roof	1.91 kPa	4.08 kPa	1.60 kPa	Roof loading does not consider ponding, etc
Design Codes:		National Building Code of Canada (NBCC 2010)			
		CSA A23.3-04			
Seismic Hazard:		NBCC Design Uniform Hazard Spectrum (2% in 50 year) for Vancouver			
		$S_a(0.2) = 0.94$; $S_a(0.5) = 0.64$; $S_a(1.0) = 0.33$; $S_a(2.0) = 0.17$			
Soil Class:		Site Class B , Vs =760 -1500 m/s (Typical of Downtown Vancouver)			
Seismic Reduction Factors:	E-W (x-Direction)	Rd=4.0 ; Ro=1.7 (Ductile Coupled Shear Wall)			
	N-S (y-Direction)	Rd=3.5 ; Ro=1.6 (Ductile Shear Wall)			
Design Wind Pressure:		q_{50} = 0.45 kPa (1 in 50 years hourly wind pressure)			
Importance Factor:	Seismic	$I_E = 1.0$			
	Wind	$I_W = 1.0$			
Concrete Strength:		35 -55MPa			
Coupling Beam:	Reinforcement	Diagonal			
	Span to Depth Ratio	~1.6 (700mm DP)			

Column Schedule

Level	f'$_c$	C6:C7 (*)	C1:C5 (*)	f'$_c$	PC1
33F-ROOF	35MPa	400 x 3000 38- 20M V. 10M @ 300 T.	400 x 1500 22- 20M V. 10M @ 300 T.		
25F-32F		400 x 3000 36- 25M V. 10M @ 400 T.	400 x 1500 22- 25M V. 10M @ 400 T.		
17F-24F	45MPa	400 x 3000 36- 25M V. 10M @ 400 T.	400 x 1500 22- 25M V. 10M @ 400 T.		
10F-16F		400 x 3000 36- 30M V. 10M @ 400 T.	400 x 1500 22- 30M V. 10M @ 400 T.		
4F-9F	55MPa	400 x 3000 36- 30M V. 10M @ 400 T.	400 x 1500 22- 30M V. 10M @ 400 T.		
P4-3F		400 x 3000 36- 35M V. 10M @ 400 T.	400 x 1500 22- 35M V. 10M @ 400 T.	35MPa	500 x 500 12- 25M V. 10M @ 400 T.

(*) See Figure 5-4, page 62 for column annotations.

Shear Wall Schedule

Level	f'c	Walls		
		SW1	SW2	SW3
25F-Roof	35MPa	600 wall 20M @ 300 HORZ. 2 layers 20M @ 300 VERT. 2 layers	300 wall 15M @ 300 HORZ. 2 layers 15M @ 400 VERT. 2 layers	600 wall 20M @ 300 HORZ. 2 layers 20M @ 300 VERT. 2 layers
10F-24F	45MPa	600 wall 20M @ 250 HORZ. 2 layers 25M @ 250 VERT. 2 layers	300 wall 15M @ 250 HORZ. 2 layers 15M @ 300 VERT. 2 layers	600 wall 20M @ 200 HORZ. 2 layers 25M @ 250 VERT. 2 layers
P3-9F	55MPa	600 wall 20M @ 200 HORZ. 3 layers 25M @ 150 VERT. 2 layers	300 wall 20M @ 200 HORZ. 2 layers 15M @ 300 VERT. 2 layers	600 wall 20M @ 200 HORZ. 3 layers 25M @ 150 VERT. 2 layers

Level	Zones		
	Z1	Z2	Z3
25F-Roof	46- 20M VERT. 10M @ 300 T. 4 legs	22- 20M VERT. 10M @ 300 T. 3 legs	42- 20M VERT. 10M @ 300 T. 4 legs
10F-24F	46- 25M VERT. 10M @ 175 T. 4 legs	22- 25M VERT. 10M @ 175 T. 3 legs	42- 25M VERT. 10M @ 175 T. 4 legs
P3-9F	58- 30M VERT. 10M @ 150 T. 4 legs	22- 30M VERT. 10M @ 150 T. 3 legs	54- 30M VERT. 10M @ 150 T. 4 legs

SW1-Z1:

Levels P3 to 9F

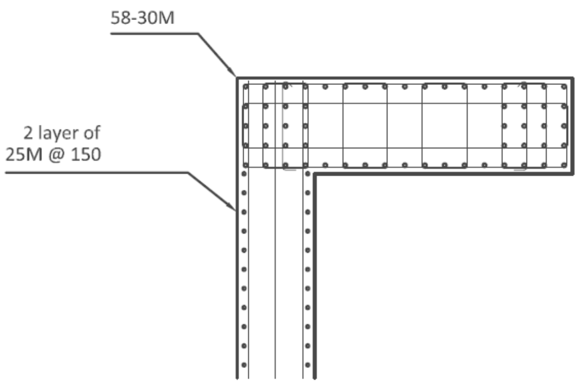

Levels 10F to 24F; 25F to Roof

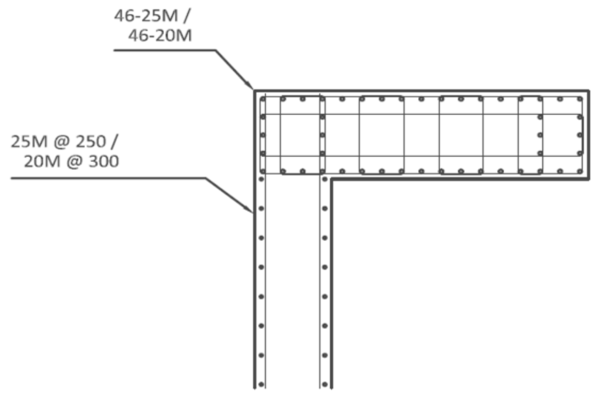

SW2-Z2:

Levels P3 to 9F

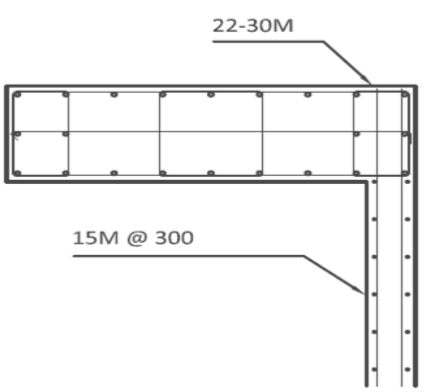

Levels 10F to 24F; 25F to Roof

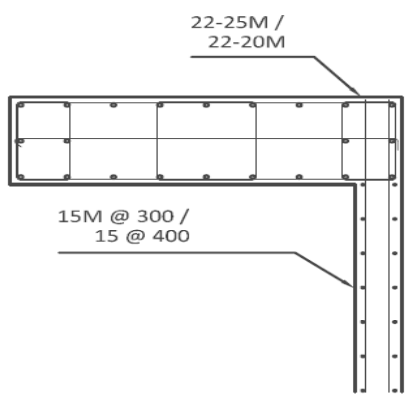

SW3-Z3:

Levels P3 to 9F

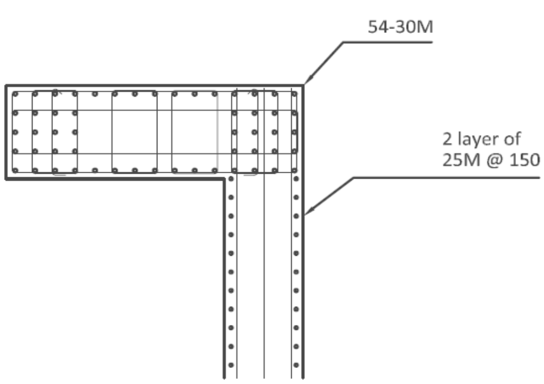

Levels 10F to 24F; 25F to Roof